Icarus 212 (2011) 42–65

Contents lists available at ScienceDirect

Icarus

journal homepage: www.elsevier.com/locate/icarus

Decadal variations in a Venus general circulation model

Helen F. Parish [a,*], Gerald Schubert [b], Curtis Covey [c], Richard L. Walterscheid [d], Allen Grossman [e], Sebastien Lebonnois [f]

[a] Institute of Geophysics and Planetary Physics, University of California, 603 Charles E. Young Dr. East, Los Angeles, CA 90095-1567, United States
[b] Department of Earth and Space Sciences, Institute of Geophysics and Planetary Physics, University of California, 595 Charles E. Young Dr. East, Los Angeles, CA 90095-1567, United States
[c] Lawrence Livermore National Laboratory, Livermore, CA 94550, United States
[d] The Aerospace Corporation, PO Box 92957, Los Angeles, CA 90009, United States
[e] Retired from Lawrence Livermore National Laboratory, Livermore, CA 94550, United States
[f] Laboratoire de Meteorologie Dynamique, CNRS, 75252 Paris, cedex 05, France

ARTICLE INFO

Article history:
Received 16 July 2009
Revised 29 October 2010
Accepted 13 November 2010
Available online 21 November 2010

Keywords:
Venus
Venus, Atmosphere
Atmospheres, Dynamics

ABSTRACT

The Community Atmosphere Model (CAM), a 3-dimensional Earth-based climate model, has been modified to simulate the dynamics of the Venus atmosphere. The most current finite volume version of CAM is used with Earth-related processes removed, parameters appropriate for Venus introduced, and some basic physics approximations adopted. A simplified Newtonian cooling approximation has been used for the radiation scheme. We use a high resolution (1° by 1° in latitude and longitude) to take account of small-scale dynamical processes that might be important on Venus. A Rayleigh friction approach is used at the lower boundary to represent surface drag, and a similar approach is implemented in the uppermost few model levels providing a 'sponge layer' to prevent wave reflection from the upper boundary. The simulations generate superrotation with wind velocities comparable to those measured in the Venus atmosphere by probes and around 50–60% of those measured by cloud tracking. At cloud heights and above the atmosphere is always superrotating with mid-latitude zonal jets that wax and wane on an approximate 10 year cycle. However, below the clouds, the zonal winds vary periodically on a decadal timescale between superrotation and subrotation. Both subrotating and superrotating mid-latitude jets are found in the approximate 40–60 km altitude range. The growth and decay of the sub-cloud level jets also occur on the decadal timescale. Though subrotating zonal winds are found below the clouds, the total angular momentum of the atmosphere is always in the sense of superrotation. The global relative angular momentum of the atmosphere oscillates with an amplitude of about 5% on the approximate 10 year timescale. Symmetric instability in the near surface equatorial atmosphere might be the source of the decadal oscillation in the atmospheric state. Analyses of angular momentum transport show that all the jets are built up by poleward transport by a meridional circulation while angular momentum is redistributed to lower latitudes primarily by transient eddies. Possible changes in the structure of Venus' cloud level mid-latitude jets measured by Mariner 10, Pioneer Venus, and Venus Express suggest that a cyclic variation similar to that found in the model might occur in the real Venus atmosphere, although no subrotating winds below the cloud level have been observed to date. Venus' atmosphere must be observed over multi-year timescales and below the clouds if we are to understand its dynamics.

1. Introduction

It is known from the earliest measurements using probes and orbiters that Venus' atmosphere is an extreme environment, with surface atmospheric pressure 92 times that on the Earth and surface temperatures around 740 K (Schubert, 1983; Seiff, 1983). Observations of Venus' atmosphere from Mariner 10 and the Venera probes (Marov et al., 1973; Murray et al., 1974) showed strong winds, with equatorial velocities more than 100 m s^{-1} just above the cloud deck. These winds are strongly superrotating, encircling the planet in around 4 Earth days, compared with the planetary body rotation period of 243 Earth days (Counselman et al., 1980; Newman et al., 1984; Rossow et al., 1990; Belton et al., 1991). Reviews of the physical and dynamical conditions of Venus' atmospheric environment include those by Gierasch et al. (1997) and Zasova et al. (2007).

Attempts have been made to determine how these strong winds are produced. It has been shown that superrotation cannot be maintained by axisymmetric processes, and eddies or other kinds

* Corresponding author.
E-mail address: hparish@ess.ucla.edu (H.F. Parish).

0019-1035/$ - see front matter © 2010 Elsevier Inc. All rights reserved.
doi:10.1016/j.icarus.2010.11.015

of waves are required to explain the observed wind structure (Hide, 1969; Schneider, 2006). Several mechanisms have been proposed to generate the measured winds and transport angular momentum from the planetary body to the equatorial atmosphere at cloud top altitudes. One suggestion, often referred to as the Gierasch–Rossow–Williams (GRW) mechanism (Gierasch, 1975; Rossow and Williams, 1979), involves the transport of angular momentum upward and poleward from the surface at low latitudes via a Hadley-type circulation, with descending motion at high latitudes. Angular momentum deposited at high latitudes at cloud top heights causes zonal jets to form and eddies, perhaps due to instabilities associated with the jets, transport angular momentum back toward the equator, producing the observed large zonal velocities at low latitudes. Many other means of producing and maintaining superrotation at cloud top heights have been suggested, for example, forcing by: thermal tides (Gold and Soter, 1969; Fels and Lindzen, 1974; Pechman and Ingersoll, 1984; Newman and Leovy, 1992; Takagi and Matsuda, 2007), the motion of the solar heating (Schubert and Whitehead, 1969), the effects of topography (Fels, 1977), planetary scale waves (Covey and Schubert, 1981; Covey and Schubert, 1982; Yamamoto, 2001), or small-scale gravity waves (Leroy and Ingersoll, 1995; Baker et al., 2000a; Baker et al., 2000b). However, the source of the observed strong superrotation is still not fully explained (see review by Gierasch et al. (1997)).

An early effort to model Venus' atmosphere produced superrotation with zonal wind magnitudes similar to those observed (Young and Pollack, 1977), but there may have been problems with the parameterization of vertical diffusion in this work (Rossow et al., 1980b; Young and Pollack, 1980). Later simulations of the Venus atmosphere in general circulation models (GCMs) tended to produce superrotation with magnitudes significantly smaller than those observed (Rossow, 1983; Del Genio et al., 1993; Del Genio and Zhou, 1996). More recent GCMs incorporating a simplified Newtonian cooling type radiation scheme (Yamamoto and Takahashi, 2003a,b, 2004, 2006; Lee et al., 2005, 2007; Herrnstein and Dowling, 2007; Hollingsworth et al., 2007) produce superrotating winds with magnitudes closer to those measured. However, unrealistically large solar heating rates in the lower atmosphere of Venus compared with the measured heating (Tomasko et al., 1980) had to be used to produce zonal wind magnitudes similar to those observed (Hollingsworth et al., 2007; Yamamoto and Takahashi, 2009). Calculations by Lebonnois et al. (2010) with realistic radiative transfer produce superrotation above around 40 km altitude, with wind magnitudes around 60–70% of those observed in cloud tracking data (Del Genio and Rossow, 1990) and comparable to those found in probe measurements (Schubert et al., 1980; Schubert, 1983). However, below around 40 km altitude, their simulated wind magnitudes are much smaller than those observed.

The superrotating cloud level winds on Venus show evidence of variability on timescales of days to years, which may be due to the influence of several different waves. Analysis of Pioneer Venus Orbiter Cloud Photopolarimeter (OCPP) ultraviolet images of cloud top winds over an interval of eight years (Del Genio and Rossow, 1990) shows that Kelvin and Rossby waves with periods around 4–5 Earth days are present; changes in the appearance of these waves suggest cyclic variability in the atmosphere on a timescale of around 5–10 years. Variability in the magnitude and structure of the cloud top winds on timescales of the order of several years is also suggested by comparisons among measurements made during different observing campaigns. Cloud top wind velocities measured during the Pioneer Venus mission (1978–1979) (Rossow et al., 1980a) show zonal winds rotating with a nearly constant angular velocity, with maximum velocities near the equator, but cloud tracking observations from Mariner 10 (Suomi, 1974; Limaye, 1977; Limaye and Suomi, 1981) 4–5 years earlier (during 1974) show prominent mid-latitude jets, as well as evidence of hemispheric asymmetry (Rossow et al., 1980a). However, due to difficulties related to the relatively low image resolution and temporal sampling, and problems with obtaining accurate wind measurements at high latitudes, these wind observations must be treated with caution (Limaye, 2007). It is also possible that the mid-latitude jets appear variable due to irregular intervals of shielding by H_2SO_4 haze layers (Moissl et al., 2009). While cloud top wind velocities provide arguable evidence of variability in Venus' atmosphere on time scales of years to tens of years or more, other observations, including the cloud top concentration of SO_2, show clear evidence of variability on a timescale of tens of years (Belyaev et al., 2008).

In this paper, we describe the results of simulations using a new model of Venus' atmospheric dynamics. Importantly, our model displays a fundamental oscillation with a 10 year timescale that might explain the observed multi-decade variability in Venus' atmosphere. Changes made to convert the Earth-based Community Atmosphere Model (CAM) to simulate Venus' atmosphere are discussed in Section 2, which also describes the physical constants and parameterizations used in the Venus CAM. The results of model simulations are presented in Section 3 and discussed in Section 4.

2. The model

We have modified the National Center for Atmospheric Research (NCAR) Community Atmosphere Model (CAM), an Earth-based climate model, to produce a new general circulation model of the Venus atmosphere (Venus CAM). We adopt the most recent version of the CAM model, which employs a finite volume dynamical core. The CAM model is a nonlinear, hydrostatic, time-dependent model which solves the primitive equations in three dimensions. The finite volume horizontal discretization is based on a conservative 'flux-form semi-Lagrangian' scheme described by Lin and Rood (1996, 1997). The time integration within the finite volume dynamics is fully explicit, using sub-cycling within the Lagrangian dynamics to stabilize the fastest wave. A full description of the CAM model is given in Collins et al. (2004). A relatively high horizontal grid resolution of 0.9° in latitude by 1.25° in longitude has been used in our simulations, with a correspondingly short dynamics timestep of 150 s. The high resolution allows us to take into account small-scale features which are important in maintaining adequate wind speeds in the relatively diffusive finite volume version of the CAM model (Jablonowski et al., 2008) and also enables us to more accurately represent the small-scale dynamical processes, eddies, and other waves that may be important in Venus' atmosphere. The vertical resolution and extent of the CAM model have been increased for Venus, from 26 levels to 50 levels, giving an upper boundary around 95 km altitude. The vertical level is given by a hybrid sigma-pressure coordinate (Simmons and Strufing, 1981). In this system, the upper regions of the atmosphere are discretized by pressure P only and lower vertical levels use the sigma (i.e., P/P_s, where P_s = surface pressure) vertical coordinate smoothly merged in, with the lowest levels being pure sigma. This allows the model to follow the features of the surface terrain, when present. The model levels have variable spacing, with a vertical grid spacing around 50 m in the lowest levels, and a spacing around 4 km near the upper boundary. In the model the pressure P at given vertical level index k, latitude index i, and longitude index j is given by $P(i,j,k) = A(k)P_0 + B(k)P_s(i,j)$, where P_0, A and B are constants. The surface pressure is set to 9.2×10^6 Pa (92 bar), decreasing to around 3 Pa at the upper boundary.

We have removed the 'physics' routines in CAM which are associated with Earth-specific processes and have retained the

'dynamics' routines which apply to any planetary atmosphere. We also include components for solving the basic primitive equations. Sufficient numerical diffusion is applied to maintain numerical stability; we use a del-squared diffusion scheme on the horizontal velocities (P. Lauritzen, private communication) with diffusion coefficient 4.9×10^5 m^2 s^{-1} in place of the standard divergence damping used in the CAM dynamical core. Del-squared diffusion, which has been used successfully in other GCMs, allows us to achieve larger wind speeds within the diffusive finite volume version of the CAM model. The CAM model uses a vertical mapping technique to provide vertical numerical diffusion rather than an explicit parameterized diffusion (Collins et al., 2004). Adjustments have also been made to change the basic parameters in CAM from Earth-like to Venus-like values (Table 1). In this simplified model, there is no topography, no diurnal or seasonal variation in the forcing, and no chemical processes.

2.1. Physics parameterizations

2.1.1. Radiation scheme

The radiation scheme originally included in the CAM model is Earth-specific and not appropriate for Venus. A simplified thermal relaxation scheme has been substituted to parameterize both the heating and cooling processes in the venusian atmosphere. The scheme is similar to those used by Lee et al. (2007), Hollingsworth et al. (2007), and Yamamoto and Takahashi (2003b). In future studies we plan to have an alternate approach available, in which heating and cooling rates are calculated using an interactive radiation treatment, based on the radiative transfer model used in the Laboratoire de Meteorologie Dynamique (LMD) Venus GCM (Eymet et al., 2009). The simplified radiation approach of this paper is a Newtonian cooling scheme in which the rate of change of temperature is proportional to the difference in temperature between the current atmospheric state and a relaxed state T_0

$$\frac{dT}{dt} = -\frac{(T - T_0)}{t_r} \tag{1}$$

where T is the current atmospheric temperature and t_r is the relaxation timescale for the heating. The relaxed state T_0, is given by a combination of a reference global mean temperature T_{ref}, which is a function of height only and an equator-to-pole temperature difference which is a function of height and latitude

$$T_0 = T_{\mathrm{ref}}(h) + T_1(h)(\cos\varphi - c) \tag{2}$$

where φ = latitude, h = vertical coordinate, c = mean value of $\cos\varphi$ over the domain, and T_1 = peak equator-to-pole temperature difference. The reference global mean temperature T_{ref} is based on Venus temperature measurements (Seiff et al., 1980; Seiff, 1983).

Fig. 1 shows the cross-section of the deviation of the applied heating from the global mean $(T_1(h)(\cos\varphi - c)/t_r$, plotted as a function of latitude, pressure, and approximate height. The relaxation timescale for the heating t_r is equal to 30 Earth days in these simulations. The radiative time constant is a strong function of altitude in Venus' atmosphere, with a factor of 10^5 variation between around 90 km altitude and the surface (Hou and Farrell, 1987). To allow for faster spin-up of the model we use a constant value for the radiative timescale, estimated from the measured values corresponding to a height around 60 km altitude, representative of the cloud top level. The value we use is in agreement with constant values used by other investigators (e.g., Hollingsworth et al., 2007; Lee et al., 2007). The global mean solar heating rate is unrealistically high below 35 km altitude compared with observations (Tomasko et al., 1980), which suggests heating rates of the order of 10^{-3} K/day. Our approximation for the lower atmosphere heating rate is consistent with values used in this part of the atmosphere in other modeling efforts (Yamamoto and Takahashi, 2003b; Hollingsworth et al., 2007; Lee et al., 2007).

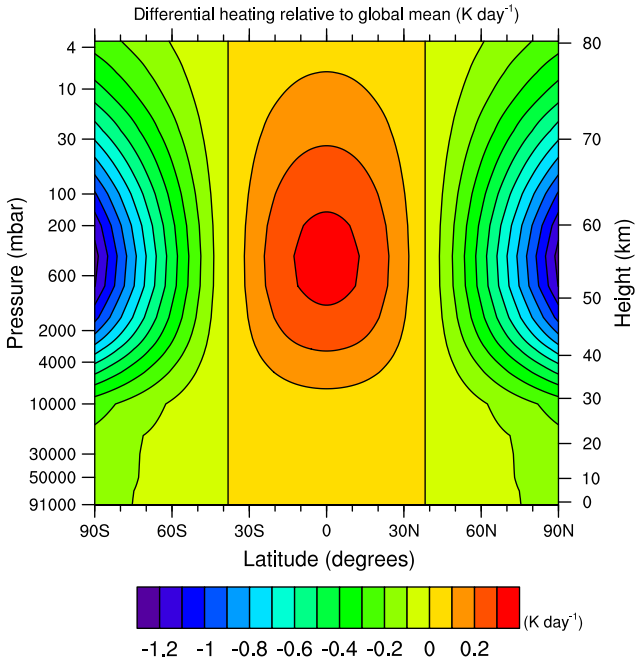

Fig. 1. Deviation of applied heating from global mean $(T_1(h)(\cos(\varphi) - c))/t_r$, where T_1 = peak equator to pole temperature difference, t_r = relaxation timescale for heating, φ = latitude, h = vertical coordinate, and c = mean value of $\cos(\varphi)$ over the domain.

Table 1
Basic properties of the model Venus atmosphere.

Planetary radius	6.052 km
Rotation period (sidereal day)	243 Earth days
Solar day	116.75 Earth days
Gravitational acceleration	8.87 m s^{-2}
Surface pressure	9.2×10^6 Pa
Molecular weight	43.45 kg k mole^{-1}
Specific heat at constant pressure	8.5×10^2 J kg^{-1} K^{-1}

2.1.2. Boundary layer schemes

2.1.2.1. Surface drag. A simple linear friction parameterization is included to represent the processes occurring near the planetary surface that transfer angular momentum between the surface and the lower atmosphere. In this scheme, the change in horizontal velocity is given by

$$\frac{d\underline{u}}{dt} = -\frac{\underline{u}}{t_f} \tag{3}$$

where t_f is the relaxation period for momentum and $\underline{u}$ is the horizontal velocity vector. This drag is applied at the lowest atmospheric level only. In these simulations a period of $t_f = 30$ Earth days has been used. The surface friction time constant of 30 days was chosen to be comparable to those used in other Venus atmosphere models (Yamamoto and Takahashi, 2003a,b; Hollingsworth et al., 2007; Lee et al., 2007).

2.1.2.2. Upper boundary sponge layer. A similar linear friction scheme is used only within the upper three levels of the atmosphere to provide a 'sponge layer' to damp any waves that might reflect from the upper boundary. The friction is of the form

$$\frac{du}{dt} = -\frac{u}{t_u} \quad (4)$$

where t_u asymptotes from around 40 days in the 3rd layer from the top to around 10 days at the upper boundary.

3. Model simulations

The simulations were run from an initial isothermal state with temperature 400 K and winds at rest. Simulations were run for 200 Earth years (around 625 Venus solar days) (in the following discussions, the term 'year' will refer to an Earth year, unless otherwise specified).

3.1. Results of simulations

3.1.1. Mean state quantities

Fig. 2 shows mean state quantities produced by the simulations after 175 simulated Earth years, time-averaged over the last 10 years. Fig. 2a shows the zonally averaged temperature, time-averaged over the 10 year interval, plotted as a function of pressure (mbar) and approximate height (km) versus latitude. The temperature maximizes around 740–750 K at the surface, dropping to near 200 K around 80 km altitude, and shows little horizontal variation near the surface. The simulated temperature structure is consistent with probe and orbiter observations (Seiff et al., 1980; Seiff, 1983).

Figs. 2b and c show, respectively, the corresponding zonally averaged zonal component of the wind (positive westward) and the meridional component of the wind (positive northward), time-averaged over the same 10-year interval. The zonally averaged zonal wind maximizes at the equator in a westward direction with magnitude over 50 m s^{-1} at the equator, around the 30 mbar level (70 km altitude). This is within the region just above the cloud tops on Venus in which the strong westward superrotating winds have been observed. The simulated wind magnitudes at this altitude are within the range of values measured by the Venera and Pioneer Venus probes (Schubert et al., 1980; Schubert, 1983) and are around 50–60% of those measured using Pioneer Venus cloud-tracking techniques (Del Genio and Rossow, 1990). At altitudes below the zonal wind maximum, wind magnitudes are significantly smaller than those observed. For example, the zonal wind speed is around 50 m s^{-1} at 50 km altitude (Schubert et al., 1980), but our simulated wind speeds at a similar altitude are less than 10 m s^{-1}. Other models also generate zonal winds at altitudes below the zonal wind maximum that are significantly smaller than those measured (e.g., Hollingsworth et al., 2007; Lebonnois et al., 2010). The magnitude of the zonally averaged zonal wind was found to slowly increase over the course of the simulation. The zonally averaged meridional wind is much smaller in magnitude, in the range of ±2 m s^{-1}. The meridional wind flows generally away from the equator in each hemisphere, just below the zonal wind maximum, with small reversals near the poles. The meridional wind magnitudes are of the same order as those measured (Counselman et al., 1980; Belton et al., 1991).

3.1.2. Time variations of zonal winds

Simulated atmospheric parameters are found to show significant variations over time. At cloud heights and above strong mid-latitude zonal jets are sometimes present, while at other times the zonal flow maximizes near the equator. The changes in the zonally averaged zonal wind over the time interval from 164 to 175 years are shown in Fig. 3. In year 164, strong westward superrotating mid-latitude jets are generated with wind speeds up to around 70 m s^{-1} centered around 65 km altitude and maximizing between ±(40 to 70) degrees latitude. Slightly smaller winds with speeds up to around 60 m s^{-1} extend all the way across the equator in the same height range. Small eastward winds with speeds up to around 10 m s^{-1} are seen below about 40 km altitude, and within the first 10 km or so above the surface there is a band of westward winds with speeds up to about 10 m s^{-1}.

In the next year, strong mid-latitude jets with wind speeds similar to those in the previous year are still seen, but the latitudes of the jet maxima have moved slightly toward the equator, to between around ±(40 to 60) degrees latitude, and the centers of the jets have moved upwards slightly to around 68 km altitude. The region of eastward winds has moved upwards in altitude and subrotating jets have developed in the altitude range of 40–50 km. The zone of westward winds near the surface has also extended upwards from the surface to around 15–20 km altitude. In the following year (166), the mid-latitude jets have become slightly weaker and have moved closer to the equator, with the jet maxima around ±40° latitude. The centers of the jets have also moved upward to around 70 km altitude. The zones of eastward and westward winds below the westward jets' maxima have also moved further upward. The eastward zonal jets at high latitudes within the band of eastward winds have peak magnitudes of around 20–25 m s^{-1}, around ±70° latitude and 40 km altitude.

Between years 167 and 170, the westward jets move toward the equator, coalesce, and decrease in magnitude to around 45–50 m s^{-1}, while maintaining the same approximate altitude around 70 km. The region of westward surface winds extends upward in height, and increases in magnitude to a maximum at the equator around 20 m s^{-1}. Over this period the region of eastward winds decreases in vertical extent. From year 168 onwards, a new region of eastward winds of around 5–10 m s^{-1} develops at the surface and expands upward to around 10 km altitude. In year 171, the region of westward winds, which was initially close to the surface, continues to move upwards in height, and the maximum westward wind moves from the equator to high latitudes forming new westward zonal jets around 70° latitude between 40 and 50 km altitude with wind speeds up to 40 m s^{-1}, comparable in magnitude with the equatorial westward jet at around 70 km altitude.

In year 172, the high altitude eastward winds have disappeared, the high latitude westward jets have intensified with wind speeds up to around 60 m s^{-1}, and the maximum of the high altitude equatorial jet has moved downwards to around 65–70 km altitude and coalesced with the region of large winds in between the high latitude westward jets. The region of small eastward winds near the surface has moved upward, and a new region of westward winds has formed at the surface. Between years 173 and 175 the high and low latitude westward jets combine to form a band of westward winds around 65 km altitude, and new westward jets develop and intensify around 50–60° latitude, reaching wind speeds of 65–70 m s^{-1}. The region of eastward winds immediately below the westward maxima, and the westward winds at the surface begin to extend upwards, and a new cycle begins. The wind structure in year 175 looks very similar to that in year 164. Similar cycles of wind variations were found to occur regularly, from around year 35 onwards, with periods of approximately 10 years.

The repeating pattern of positive and negative westward winds, combined with the upward motion of these layers over time, suggests that the regions of zonal winds of alternating sign represent different phases of an upward moving oscillation with a period close to 10 years. The movement of the zonal wind maxima from high latitudes to the equator and back occurs in combination with the apparent upward moving oscillation.

3.1.3. Time variations of meridional winds

The zonally averaged meridional wind (positive northward) is shown in Fig. 4. The meridional wind shows a general pattern of

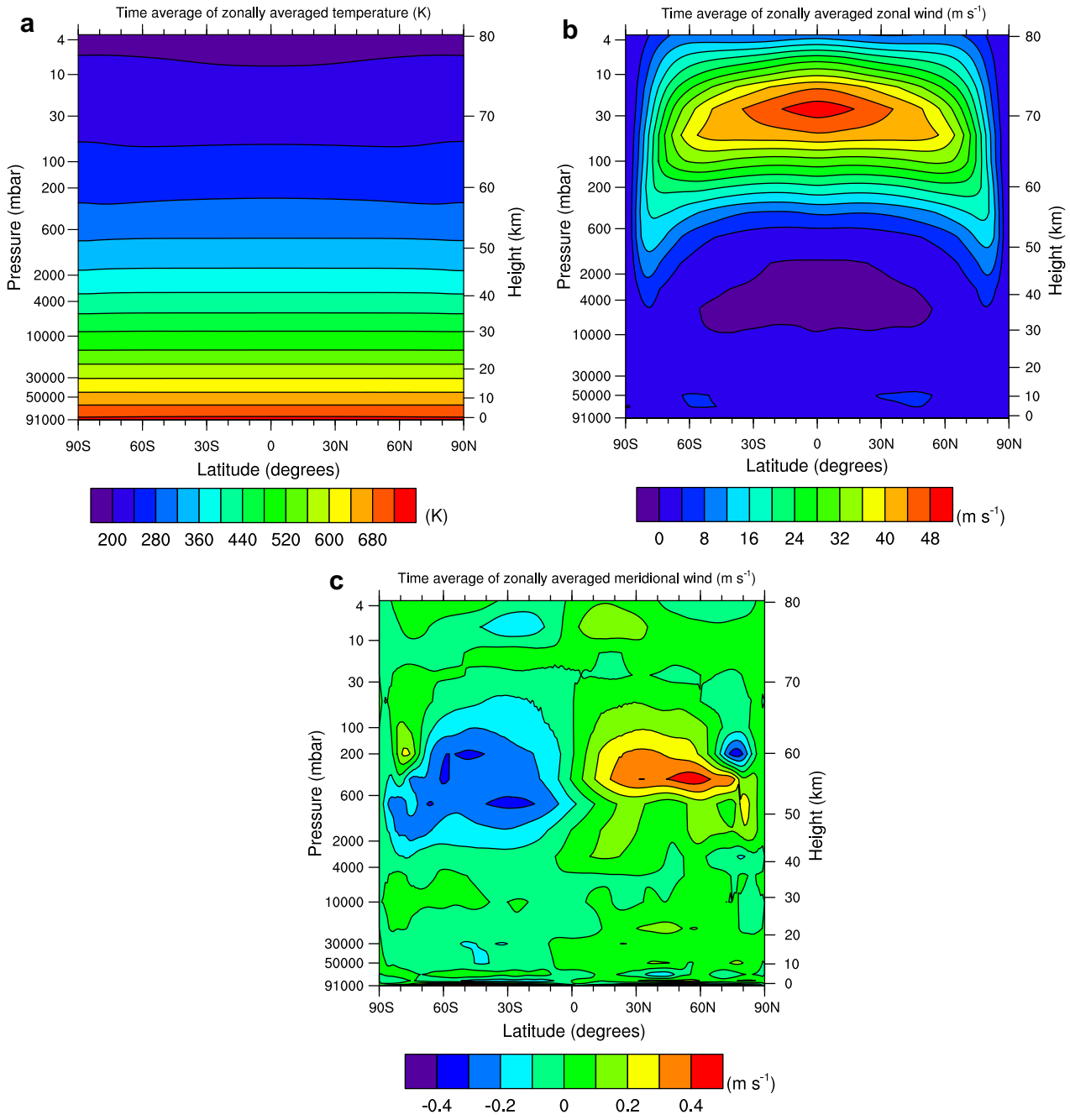

Fig. 2. (a) Zonally averaged temperature, time-averaged over years 165–175. (b) Zonally averaged zonal wind (positive westward), time averaged over years 165–175. (c) Zonally averaged meridional wind (positive northward), time-averaged over years 165–175.

poleward winds in each hemisphere between the surface and around 60 km altitude, with peak magnitudes occurring in the 45–65 km altitude range. At times there appears to be a largely Hadley-type circulation between the ground and around 65 km altitude, for example in years 168, 172, and 175, although in these years some meridional wind reversals are seen below 40 km altitude. At other times there are several meridional wind reversals between the surface and around 40 km altitude, for example in years 164, 165, 167, 173, and 174. The circulation is not well explained as a simple large scale Hadley circulation.

Above the meridional wind maxima at around 65 km altitude the meridional flow tends to be reversed relative to the basically poleward circulation below. Above 65 km altitude there is either a single cell in each hemisphere in which the meridional wind is reversed, for example in years 173 or 174, or there are multiple meridional wind reversals, for example in years 170 or 171. The meridional transport appears to account for the waxing and waning of the zonal jets. For example, in year 171 the meridional wind shows a mostly poleward flow between 40 and 70 km altitude, as the prograde zonal jets are strengthening. In year 172 the poleward flow around 60 km altitude encounters a strong reversed equatorward flow at high latitudes, which may account for the narrowing of the jet width at high latitudes. The meridional flow acts to reduce the magnitude of the prograde flow and move it more toward the equator, as seen in year 174. The meridional wind structure can be seen to move upward, for example in years 164–166, consistent with the upward motion of the zonal winds during the same period. There is an approximately 10 year variation in the meridional

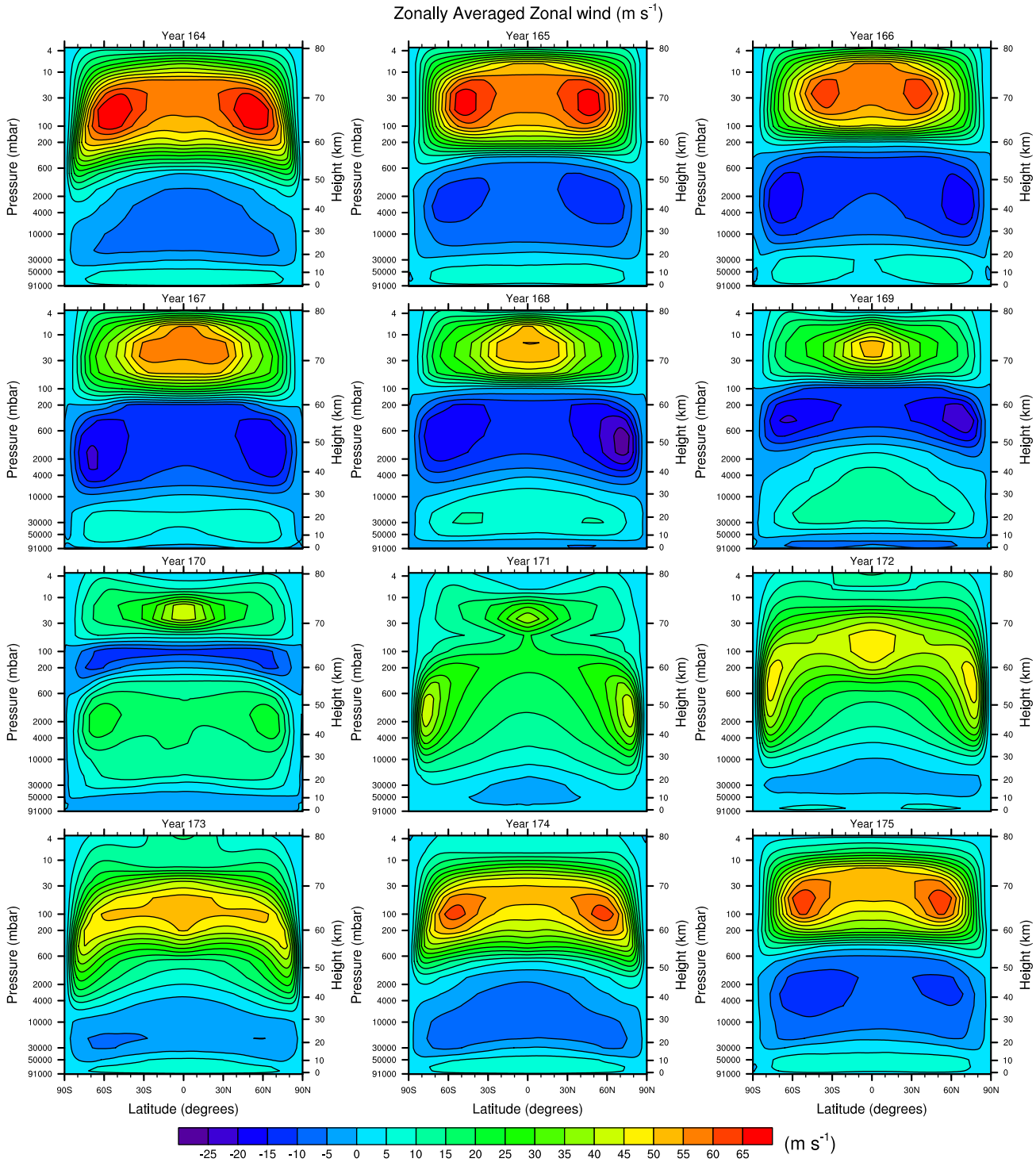

Fig. 3. Changes in zonally averaged zonal wind over the time interval 164–175 years.

winds, with a period similar to that found in the zonal winds, as can be seen in the similarities in structure between years 164 and 174 and years 165 or 166 and 175.

3.1.4. Comparison of time variation of zonal winds with observations

We examine the time variation of the zonally averaged zonal winds at cloud top heights in our simulations and compare them with observations. Simulated winds are shown for an altitude around 70 km at the equator in Fig. 5, for the time interval from year 164 to 175. This can be compared with time variations of the zonal winds at cloud top heights at the equator from measurements by the Pioneer Venus Orbiter Cloud Photopolarimeter instrument (OCPP) (Limaye et al., 1988; Rossow et al., 1990), as given in Del Genio and Rossow (1990). In Fig. 6 of Del Genio and Rossow (1990), zonal winds are shown for the time interval of 7 years between 1979 and 1985.

The observed zonal winds show a variation in magnitude over this interval, with values around 96 m s^{-1} in 1979, falling to 88 m s^{-1} in 1982, and increasing to 97 m s^{-1} in 1985. The average magnitude of our superrotating cloud top winds is smaller than the

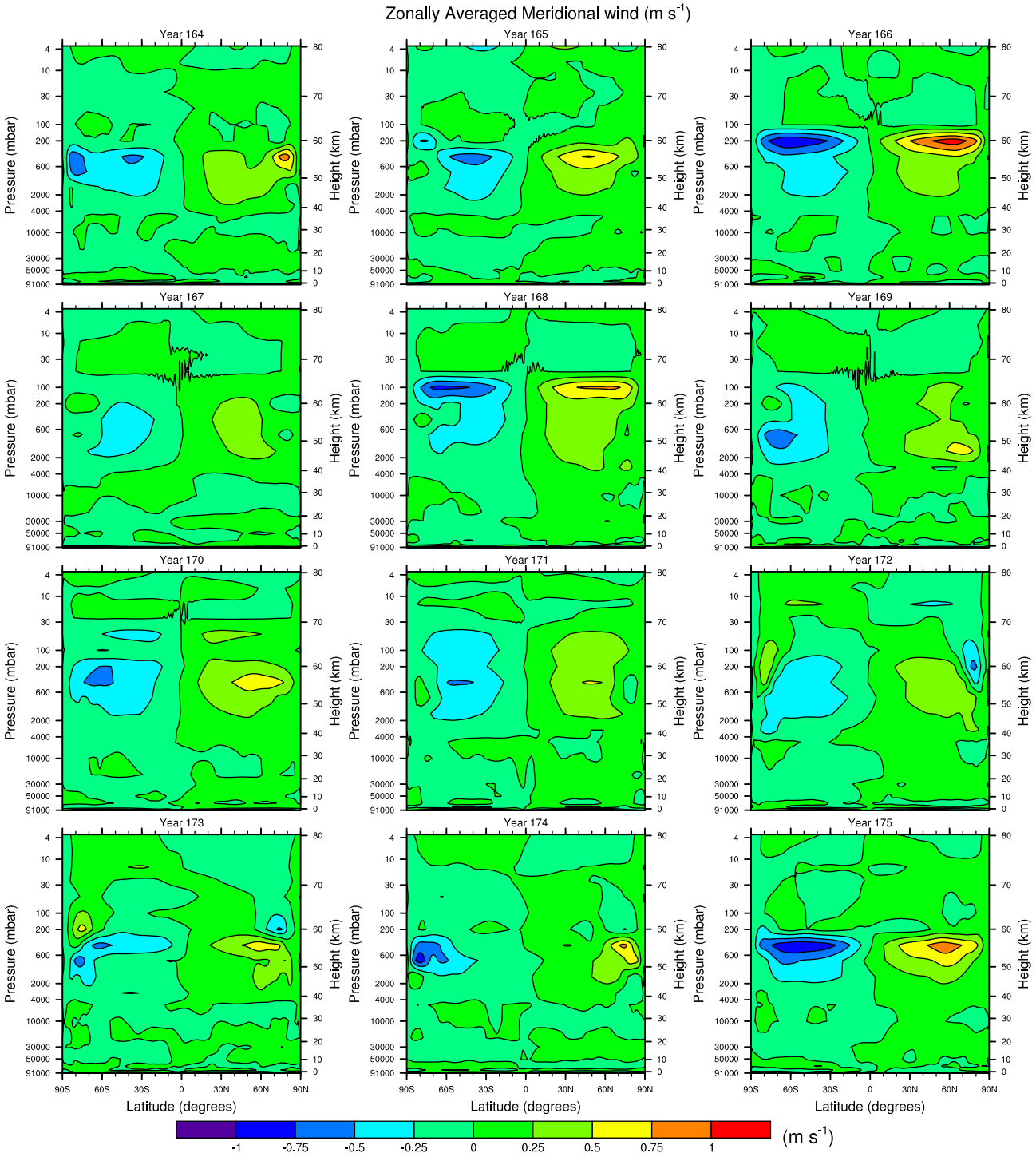

Fig. 4. Changes in zonally averaged meridional wind over the time interval 164–175 years.

observed winds by around 40 m/s at cloud top heights. The zonal wind velocity in our simulations varies between around 57.5 and 37.5 m s^{-1}, giving a peak to peak amplitude of around 20 m s^{-1}. Insufficient measurements are available to determine whether the observed cloud-tracking wind variation involves a single fluctuation of wind magnitude or a periodic variation. If the variation in the observed winds is periodic then the peak to peak amplitude of the oscillation, of around 9 m s^{-1}, is around half the magnitude of the oscillation found in our simulations, and the period associated with the observed variation is around 6–7 years rather than the approximately 10 years we find in our simulations. The observations therefore suggest the possible presence of a periodic oscillation in the zonal winds at cloud top heights with a slightly smaller amplitude than the one we find in our simulations and a period of several years.

3.1.5. Height versus time cross-sections

The propagation of the simulated long period oscillations is investigated in Fig. 6, which shows the zonally averaged zonal wind minus the time average of the zonally averaged zonal wind. We have subtracted the time independent background zonally averaged zonal wind to focus on the oscillations. Results are

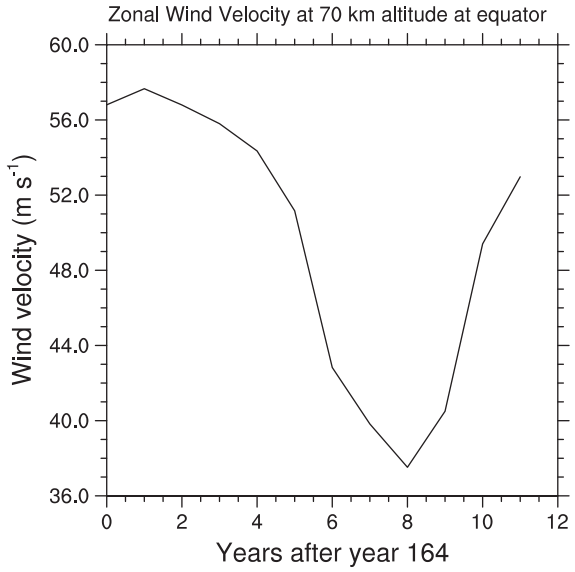

Fig. 5. Time variation of zonal winds at 70 km altitude at the equator.

plotted as a function of pressure and height versus time at the equator and 65° latitude, for the interval 155–200 years.

The series of sloping maxima and minima between the surface and 80 km altitude shows the presence of an oscillation. The maxima and minima move upwards in altitude with time, and increase in amplitude with increasing height, consistent with an upward traveling oscillation. The oscillation is present at all latitudes. Maximum velocities occur between ~55 and 65 km altitude, at the equator and at higher latitudes, with smaller maxima around 75–80 km altitude at the equator, just above the time-averaged peak zonal wind at the equator, at 70 km altitude (see Fig. 2b). The oscillation has a similar vertical length scale of about 80–100 km at both low and high latitudes. Above the magnitude peak the oscillation is strongly dissipated.

There may be a small amount of reflection from the upper boundary which is difficult to completely eliminate within computer simulations. Above the height of the peak zonal wind magnitude, there is a small reverse tilt in the wind variations, although the oscillation tends to become evanescent above the height of the magnitude peak. Oscillations travel upward from the lower boundary, with an approximately 10 year period, but there are no corresponding oscillations descending down to the lower boundary. If there is reflection at the upper boundary it does not produce these upward propagating periodic oscillations which are generated at the lower boundary, most likely by instabilities at or near the surface. We note that the oscillations we see here are not the same as the quasi-biennial oscillations (QBO) found in the Earth's atmosphere (Andrews et al., 1987; Baldwin et al., 2001), which also show a progression of phase with height over time. The phases of the periodic variations we see here ascend in altitude with time as opposed to the descending phase fronts characteristic of the QBO, which are driven downward by the interaction of the mean flow with vertically propagating gravity waves and large scale equatorial waves (Andrews et al., 1987).

3.2. Spectra

Spectra of the zonal wind at a given altitude and latitude calculated using fast Fourier transform analysis are shown in Fig. 7 for the time interval from year 155 to 200 at longitude 180° with a one year resolution. The spectra at a height of 65 km at the equator and at 65° latitude are shown in Fig. 7a and b, respectively. Fig. 7c and d show the spectra at the surface for the equator and 65° latitude, respectively. At all altitudes and latitudes, there is a dominant period around 10 years. There are also significant smaller spectral peaks at periods around 5 years and 2–3 years, which may be harmonics of the main periodicity.

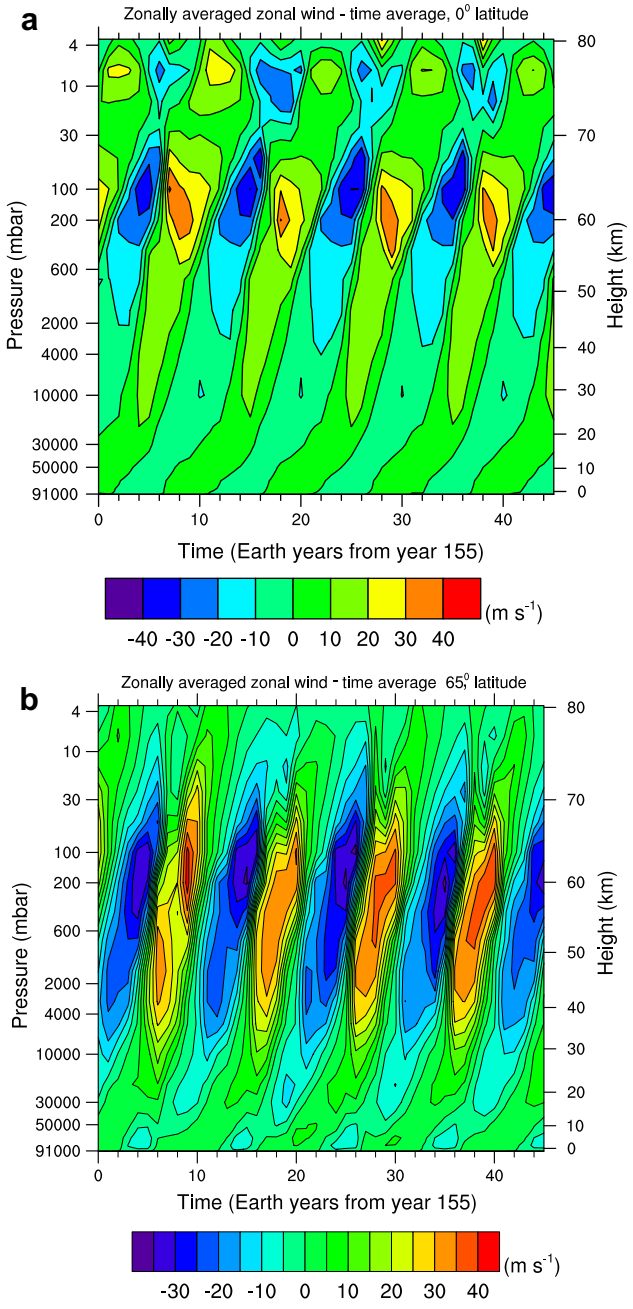

Fig. 6. (a) Zonally averaged zonal wind minus time average of zonally averaged zonal wind for the time interval 155–200 years, at the equator. (b) Zonally averaged zonal wind minus time average of zonally averaged zonal wind for the time interval 155–200 years, at 65° latitude.

The exact nature of the long period oscillations we find in our simulation is somewhat uncertain. However, initial investigations have determined that the oscillation shows considerable zonal symmetry as well as evidence of overturning in the levels close to the surface. Atmospheres with slow rotation rates may be unstable to symmetric perturbations, where the condition for a symmetric instability is given by $f^2(1 - 1/Ri) - fdU/dy < 0$ (Andrews et al., 1987), where U = zonally averaged zonal wind, y = latitudinal distance, f = Coriolis parameter = $2\omega\sin(lat)$,

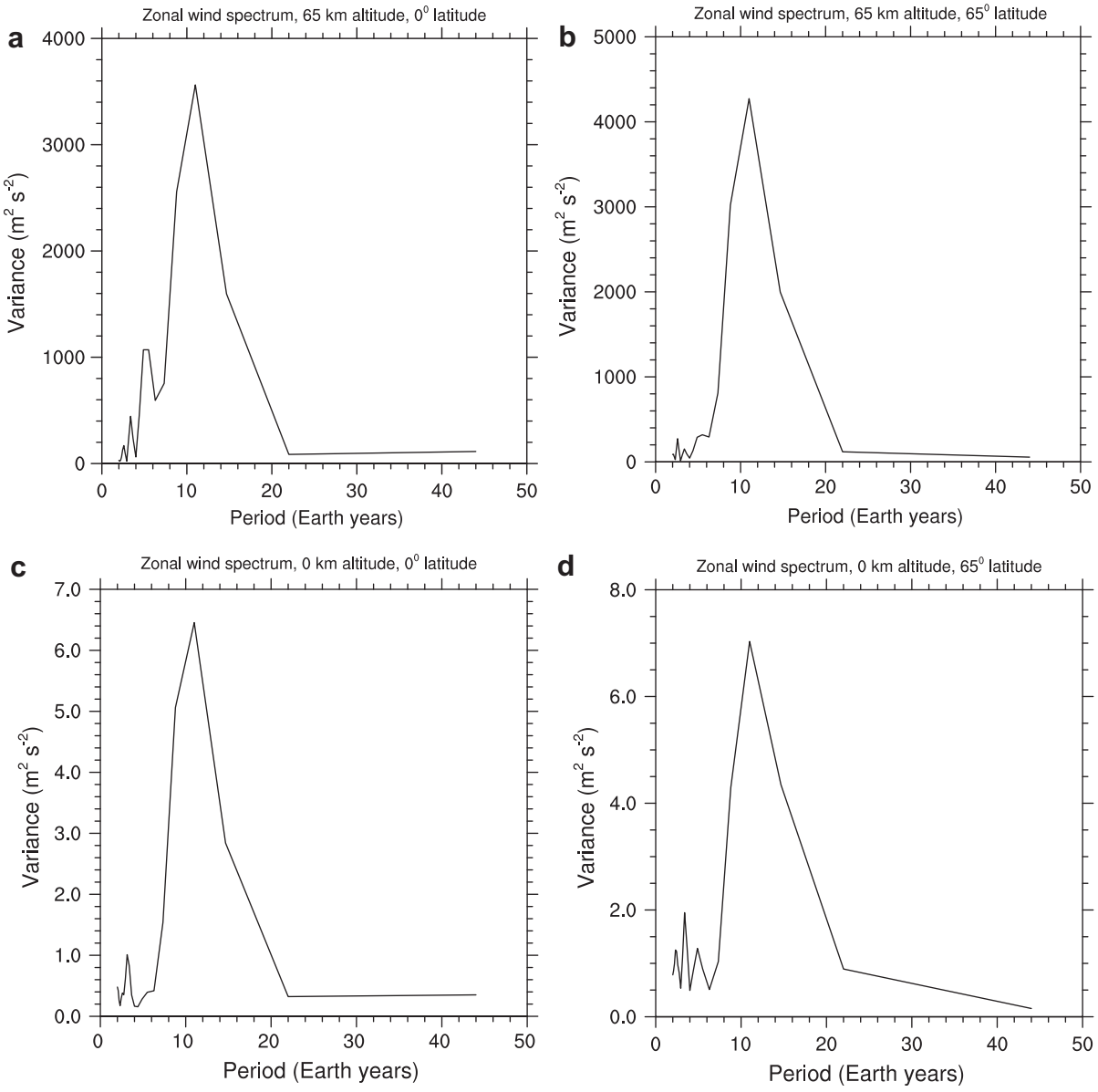

Fig. 7. Spectra of zonal wind for the time interval 155–198 years, with one year time resolution: (a) at 65 km altitude and 0° latitude (b) at 65 km altitude and 65° latitude (c) at 0 km altitude and 0° latitude (d) at 0 km altitude and 65° latitude.

ω = planetary rotation rate, lat = latitude, and Ri = Richardson number. This equation approximates to $f - dU/dy < 0$ for large Ri, which applies at the surface. We find that the condition for a symmetric instability is satisfied at low latitudes at the surface, as illustrated for year 164 in Fig. 8.

It is possible that an instability at the surface, combined with a long period overturning, might excite the periodic oscillations we find. A possible scenario would be an internal cycle excited by a symmetric instability near the surface and propagated and modulated by the interplay of the mean zonal flow and the horizontal and vertical transports of momentum. The condition for symmetric instability is the same as that for inertial instability for the conditions that apply near the surface within our simulations. Inertial instabilities were also found by Joshi and Young (2002) in their simulations of Venus' atmosphere, and were found to be associated with wind oscillations with timescales of decades, with periods of the order of 200 Venus days, or 60–70 Earth years. Their model and parameterizations differ from ours in that their model is two-dimensional, uses latitudinally asymmetric surface heating, and their timescale for thermal relaxation at the lower boundary is 30 Earth years compared with our 30 day relaxation timescale. However, the fact that they also find oscillations with periods of the order of decades related to inertial instabilities lends support to the results we report here and suggests that Venus' atmosphere may be susceptible to inertial instabilities and to oscillations with periods of the order of decades. The oscillation is also found to have characteristics of a vacillation cycle with a periodic exchange in momentum between high and low latitudes (see Webster and Keller, 1975). Further investigations will be performed to determine the nature of the eddy processes (whether barotropic or baroclinic) and whether the observed oscillation is connected with a symmetric instability or with another process, perhaps related to atmospheric overturning near the surface.

3.2.1. Global angular momentum

The global relative angular momentum (the angular momentum of the global atmosphere relative to the solid body of the planet) is shown from the beginning of the simulation to year

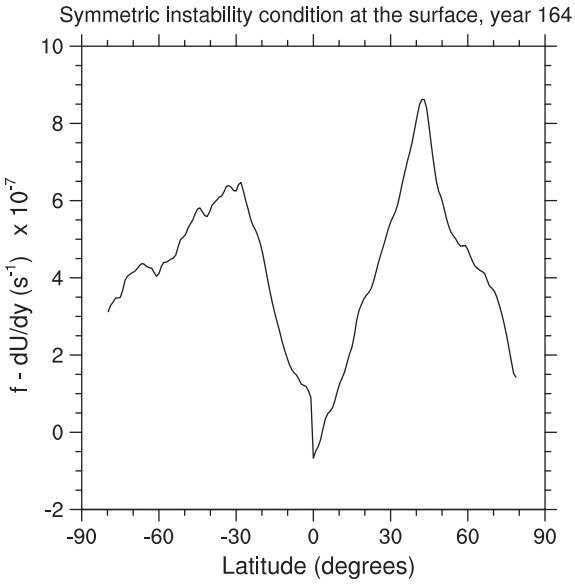

Fig. 8. Symmetric instability condition as a function of latitude at the surface in year 164.

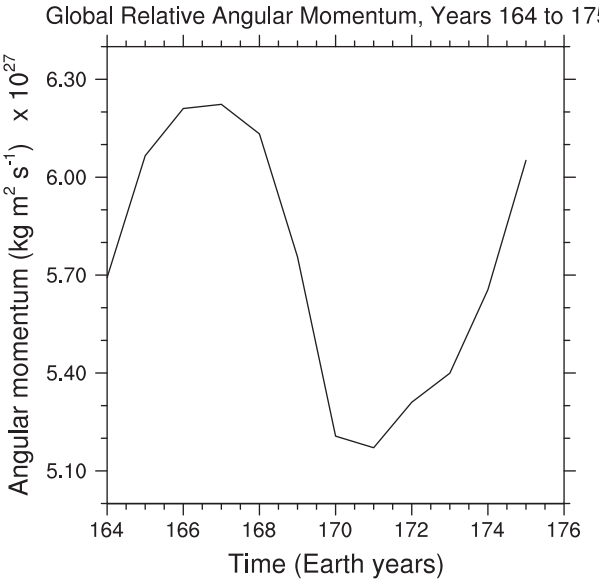

Fig. 10. Global relative angular momentum versus time, between years 164 and 175.

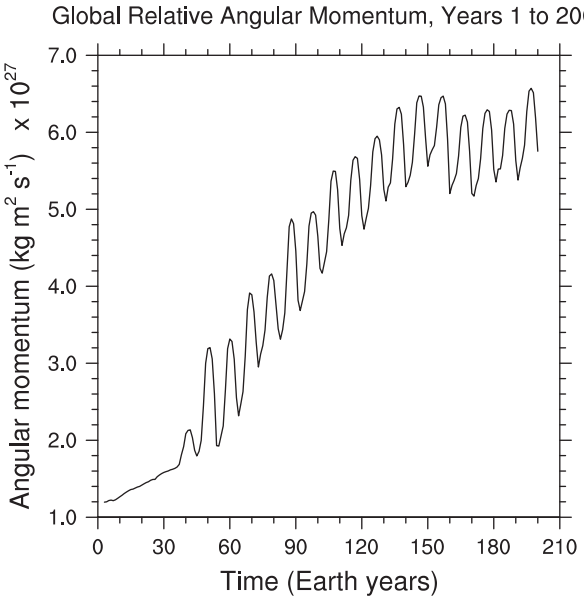

Fig. 9. Global relative angular momentum versus time, between years 1 and 200.

200 in Fig. 9. The global angular momentum of the atmosphere relative to the solid planetary body is always positive, indicating that the zonal winds generated in the simulations are superrotating. The overall angular momentum increases steadily over time and levels off after around 150 years, suggesting that some kind of equilibrium is reached in the atmosphere. After about year 35 a strong oscillation, superimposed on the gradual increase of the global relative angular momentum, sets in with a period (about 10 years) similar to that seen in the zonal wind variations and the wind spectra. The variation in the angular momentum over a single cycle is plotted in Fig. 10, for years 165–175. Comparison of Figs. 10 and 3 shows that when the global relative angular momentum maximizes, around year 167, the zonal wind adjacent to the planetary surface is a maximum in a positive (westward) direction. The angular momentum starts to decrease when the winds in the layer immediately next to the surface turn in the eastward direction in year 168. The angular momentum continues to decrease up to year 171. In year 172, the wind closest to the surface has turned westward and the angular momentum begins to increase again. Thus, the global angular momentum is related to the phase of the upward propagating oscillation at the surface. The winds closest to the surface have the most significant effect on the magnitude of the global angular momentum since the majority of the mass of the atmosphere is concentrated close to the surface. We describe our analyses of the transport of angular momentum in our simulations in the next section.

3.2.2. Angular momentum transport

3.2.2.1. Fluxes.

3.2.2.1.1. Meridional transport.

3.2.2.1.1.1. Northward flux of zonal angular momentum due to time-mean meridional cells. Fig. 11 shows zonal mean cross-sections of the northward flux of zonal angular momentum due to time-mean meridional cells (in $m^2\,s^{-2}$), given by $[\langle u\rangle][\langle v\rangle]$, where u = westward wind velocity, v = northward wind velocity, $[u]$ denotes a zonal average of u, and $\langle u\rangle$ denotes a time average of u (see e.g., Peixoto and Oort, 1992). The time mean values are averages of monthly values within a given year. Values are plotted as a function of pressure and height versus latitude, for the 12 year time interval from year 164 to 175.

The largest values of the momentum flux are generally seen between around 40 and 60 km altitude. During years 170–172 between around 40 and 55 km altitude the zonal winds are positive (westward) in both hemispheres (see Fig. 3) and the meridional winds are poleward in each hemisphere (see Fig. 4). The meridional flux of zonal angular momentum is positive in the northern hemisphere in this height range, associated with positive (westward) winds and positive (northward) winds. In the southern hemisphere, the meridional flux of zonal angular momentum is negative, corresponding to positive westward winds and negative southward winds. These fluxes represent a buildup of momentum in the westward zonal jets at middle to high latitudes, with motion away from the equator in both hemispheres, as seen in the zonal wind panel in Fig. 3. An upward motion of the momentum flux peaks is also seen, corresponding to the upward movement of the zonal wind jets (Fig. 3).

During years 165–169, between around 45 and 65 km, there are predominantly eastward zonal winds, associated with northward

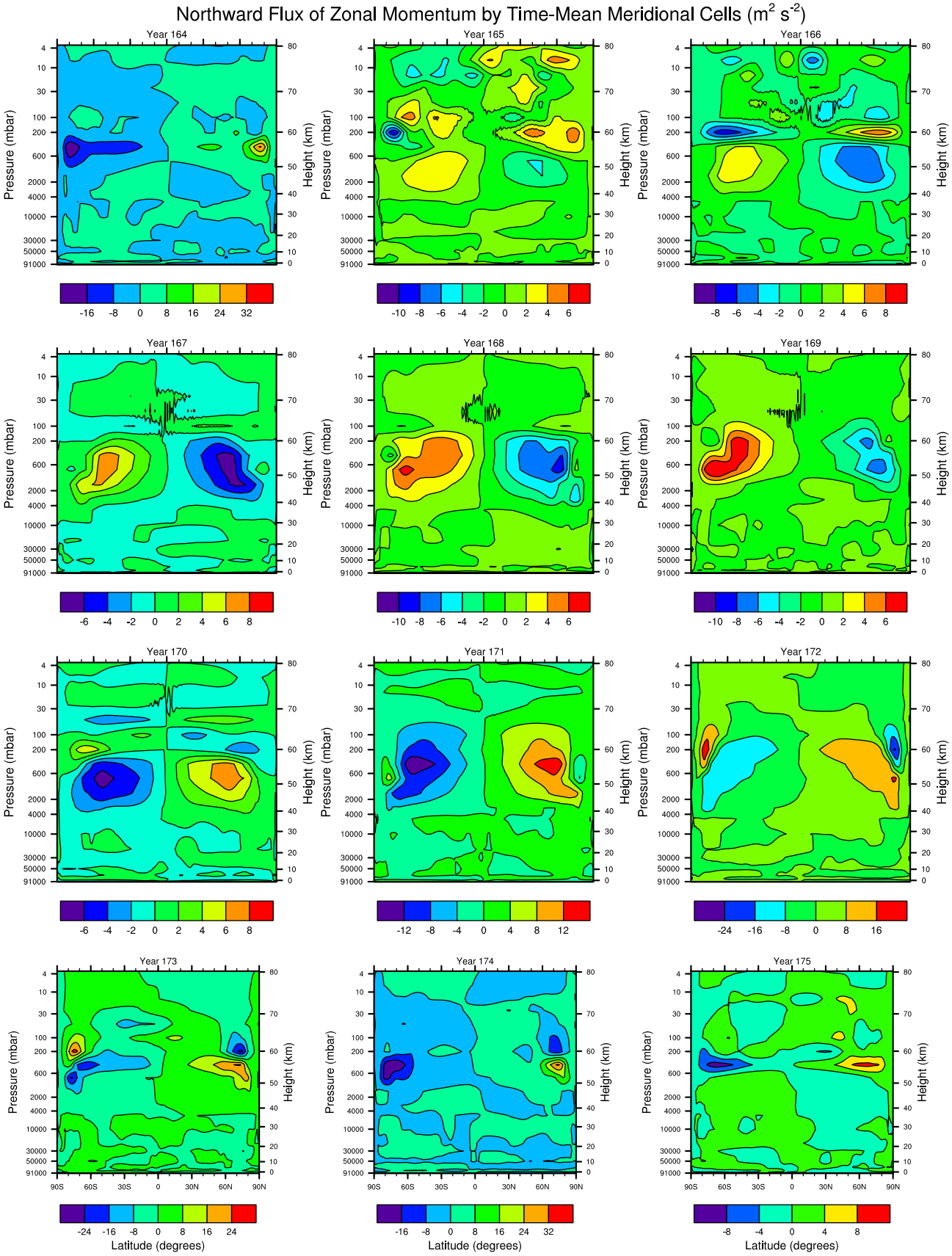

Fig. 11. Zonal mean cross-sections of the northward flux of zonal angular momentum due to time-mean meridional cells ($m^2\ s^{-2}$).

winds in the northern hemisphere and southward winds in the southern hemisphere, giving a negative flux of zonal angular momentum in the northern hemisphere and a positive flux of zonal angular momentum in the southern hemisphere. This corresponds to a buildup of eastward jets at high latitudes between years 165 and 169 in this altitude range, as can be seen in Fig. 3, with movement away from the equator in both hemispheres. An upward motion of the momentum flux peaks is also seen in this interval, corresponding to the upward movement of the eastward jets seen in Fig. 3. Below around 40 km altitude the meridional flux shows a more complicated structure, with several reversals of direction corresponding to the reversals in the meridional wind (Fig. 4). Between years 169 and 170 the zonal winds around 50 km altitude reverse from eastward to westward, as the decadal oscillation in the zonal wind moves upward. The sign of the northward flux therefore reverses between years 169 and 170 at this altitude. The region between 50 and 60 km altitude in year 169 in which the zonal winds are eastward has reduced in vertical extent and moved upward to around 60 km altitude in year 170, and disappears in year 171 when the zonal winds are all westward at these altitudes. In years 172 and 173, a reversal of the momentum flux is seen close to the poles around 60 km altitude, which is associated with a movement of the westward zonal wind jets from very high latitudes back toward the equator. The momentum flux variations in Fig. 11 also show evidence of an approximately 10 year periodicity, displaying similarities in structure between year 164 and years 174 to 175.

3.2.2.1.1.2. Northward flux of zonal angular momentum due to transient eddies. The zonal mean cross-sections of the northward flux of zonal angular momentum due to transient eddies for the same time interval are displayed in Fig. 12. The flux due to eddies is given by $[u'v']$ (in $m^2\ s^{-2}$), where u' denotes $u - \langle u \rangle$ (Peixoto and Oort, 1992).

The flux due to eddies is of similar magnitude or a few times smaller than the flux due to time-mean meridional cells. The flux due to stationary perturbations is generally around an order of magnitude less than that due to transient eddies and is not shown here. The flux due to transient eddies generally tends to oppose the flux due to time-mean meridional cells. For example, in years 167–169 between around 40 and 55 km altitude where there are eastward zonal wind jets, the meridional flux of momentum due to eddies is in the opposite direction and peaks at slightly higher latitudes than the flux peaks in the same altitude range due to time-mean meridional cells, and tends to transfer momentum toward the equator. The flux peaks can also be seen to move upward with the upward motion of the zonal wind jets. Similarly, around 50–60 km altitude in years 164–166, the momentum flux associated with the westward zonal jets due to eddies opposes the momentum flux due to time-mean meridional cells, and tends to drive the wind maxima back toward the equator. The momentum flux due to eddies also follows the upward motion of the westward zonal jets. Below 40 km altitude the flux due to transient eddies also transports angular momentum toward the equator for both westward and eastward winds. For example, in year 167 the eddy momentum fluxes (Fig. 12) are of opposite sign above and below 30 km, corresponding to the eastward winds above 30 km and westward winds below. In both cases this indicates transport of angular momentum back toward the equator. In years 168 and 169, a region of eastward winds has started to appear near the surface below the westward winds (see Fig. 3). A corresponding band of flux of opposite sign appears near the surface (see Fig. 12), again indicating transport of angular momentum back toward the equator.

3.2.2.1.2. Vertical transport.

3.2.2.1.2.1. Vertical flux of zonal angular momentum due to time-mean meridional cells. Fig. 13 shows zonal mean cross-sections of the vertical flux of zonal angular momentum per unit mass due to time-mean meridional cells, given by $-H[\langle u \rangle][\langle w \rangle]/p$ (in $m^2\ s^{-2}$), where w = vertical velocity in pressure coordinates ($=dp/dt$ where t is time), p = pressure, H = scale height, for the time interval from year 164 to 175. The flux in pressure coordinates has been multiplied by $-H/P$ to give quantities approximately in terms of the vertical velocity in physical height coordinates (dz/dt, where z is height) rather than in pressure coordinates.

The vertical fluxes due to time-mean meridional cells are significantly smaller than the corresponding horizontal fluxes. Within around ±40° latitude of the equator the vertical flux of zonal momentum is generally positive in regions where the zonal winds are westward (positive) and negative where the zonal winds are eastward (negative), corresponding to the upward (positive) vertical winds in this latitude range, and an upward motion of zonal angular momentum. For example, in years 170–172 between around 40 and 50 km altitude, where zonal winds are generally westward, there is a positive flux at low latitudes, corresponding to upward vertical winds. These regions of positive fluxes move upward as the westward zonal wind moves upward in years 170–172 (see Fig. 3). Similarly in years 167–169 between 40 and 50 km altitude for latitudes less than 40°, the fluxes are negative, corresponding to eastward (negative) winds and upward (positive) vertical winds, corresponding to an upward motion of zonal angular momentum at low latitudes in these years. Below 40 km altitude there is also a generally upward motion of angular momentum within around ±40° latitude of the equator (fluxes are positive where zonal winds are westward and negative where zonal winds are eastward). However, below 40 km within this latitude range, the circulation appears more complex, with small regions of downward motion of angular momentum within the regions of overall upward motion. At latitudes higher than 40°, there is a generally downward vertical wind, giving positive fluxes in the regions of negative (eastward) winds and negative fluxes in the regions of positive (westward) winds. For example, in years 170–172 negative fluxes are seen at latitudes above around 40° between around 40 and 60 km altitude, corresponding to westward (positive) zonal winds and downward (negative) vertical winds, giving a downward motion of zonal angular momentum. Below around 40 km altitude at high latitudes there are also generally downward vertical winds and downward motion of angular momentum, with small regions of upward movement within the regions of overall downward motion.

3.2.2.1.2.2. Vertical flux of zonal angular momentum due to transient eddies. Fig. 14 shows zonal mean cross-sections of the vertical flux of momentum per unit mass due to transient eddies for years 164–175, where the eddy flux is given by $-H[u'w']/p$.

The vertical fluxes due to transient eddies are significantly smaller than the corresponding horizontal fluxes. The vertical fluxes due to transient eddies also tend to be smaller than the vertical fluxes due to time-mean meridional cells. The vertical fluxes due to eddies are generally largest at high latitudes, where they tend to act in the opposite direction to the time-mean fluxes and they show variations with approximately the same 10 year period as the zonal wind variations. The peak fluxes show upward motion consistent with the upward movement of the zonal wind structure. The flux due to stationary perturbations is generally around an order of magnitude smaller than that due to eddies and is not shown here.

The regions of upward motion of westward momentum at low latitudes and downward motion at higher latitudes in combination with the meridional fluxes illustrated in Fig. 11 suggest the presence of a simple Hadley-type circulation within the altitude region where the mid-latitude jets form, where the vertical fluxes at low latitudes due to time-mean meridional cells transports angular momentum to higher altitudes and meridional fluxes transport angular momentum toward the poles. The effects of waves,

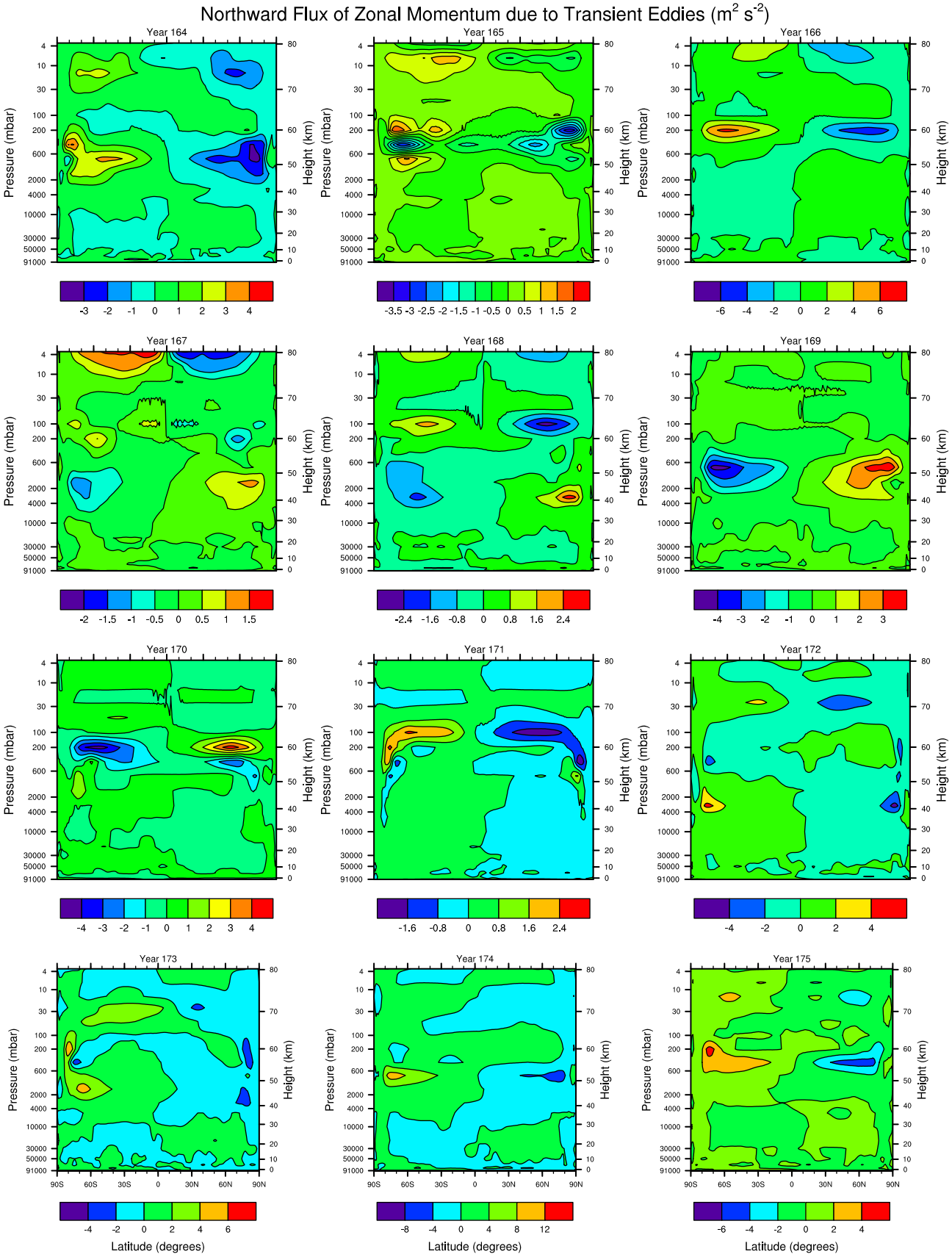

Fig. 12. Zonal mean cross-sections of the northward flux of zonal angular momentum due to transient eddies (m^2 s^{-2}).

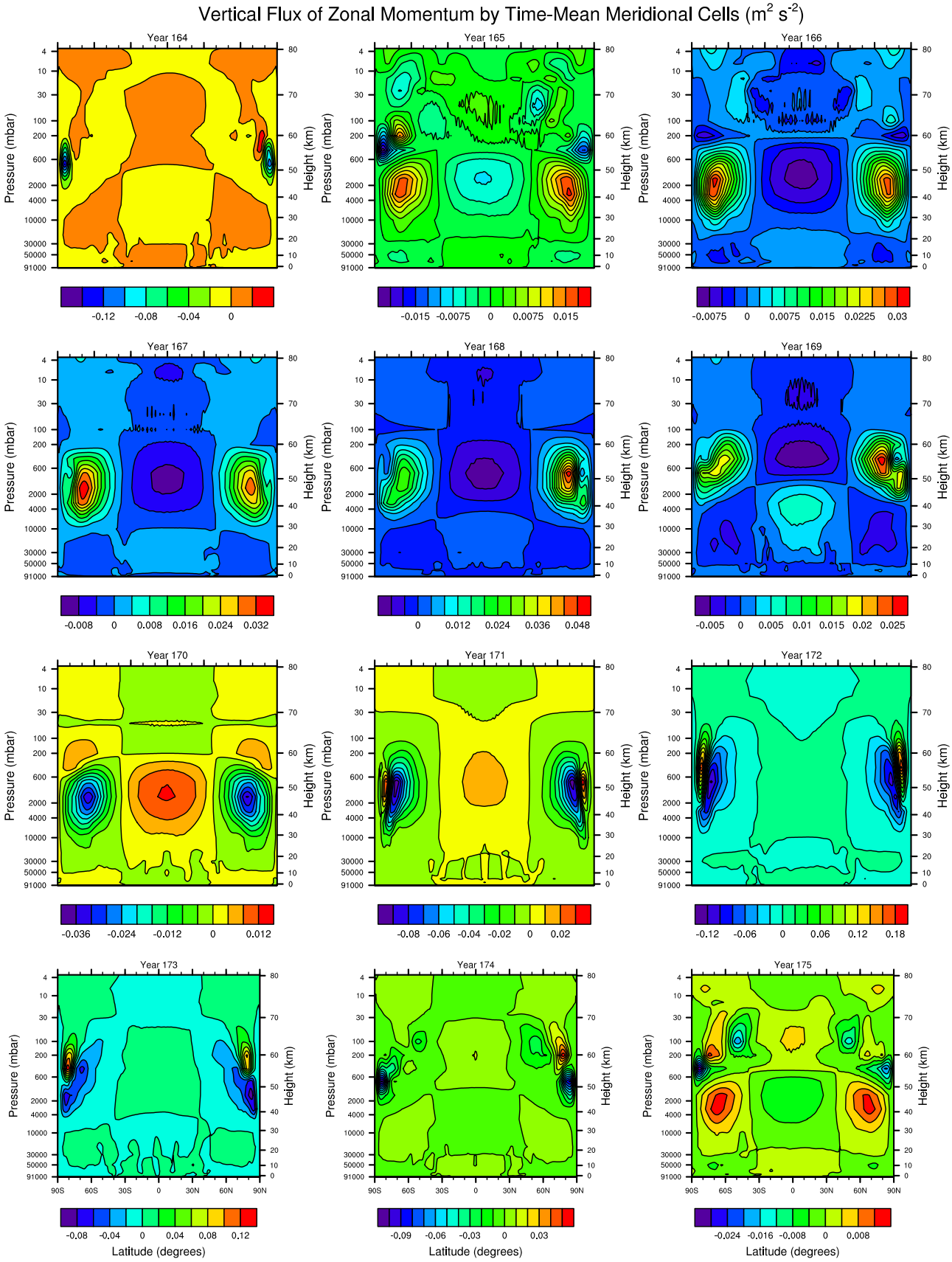

Fig. 13. Zonal mean cross-sections of the vertical flux of zonal angular momentum due to time-mean meridional cells ($m^2\ s^{-2}$).

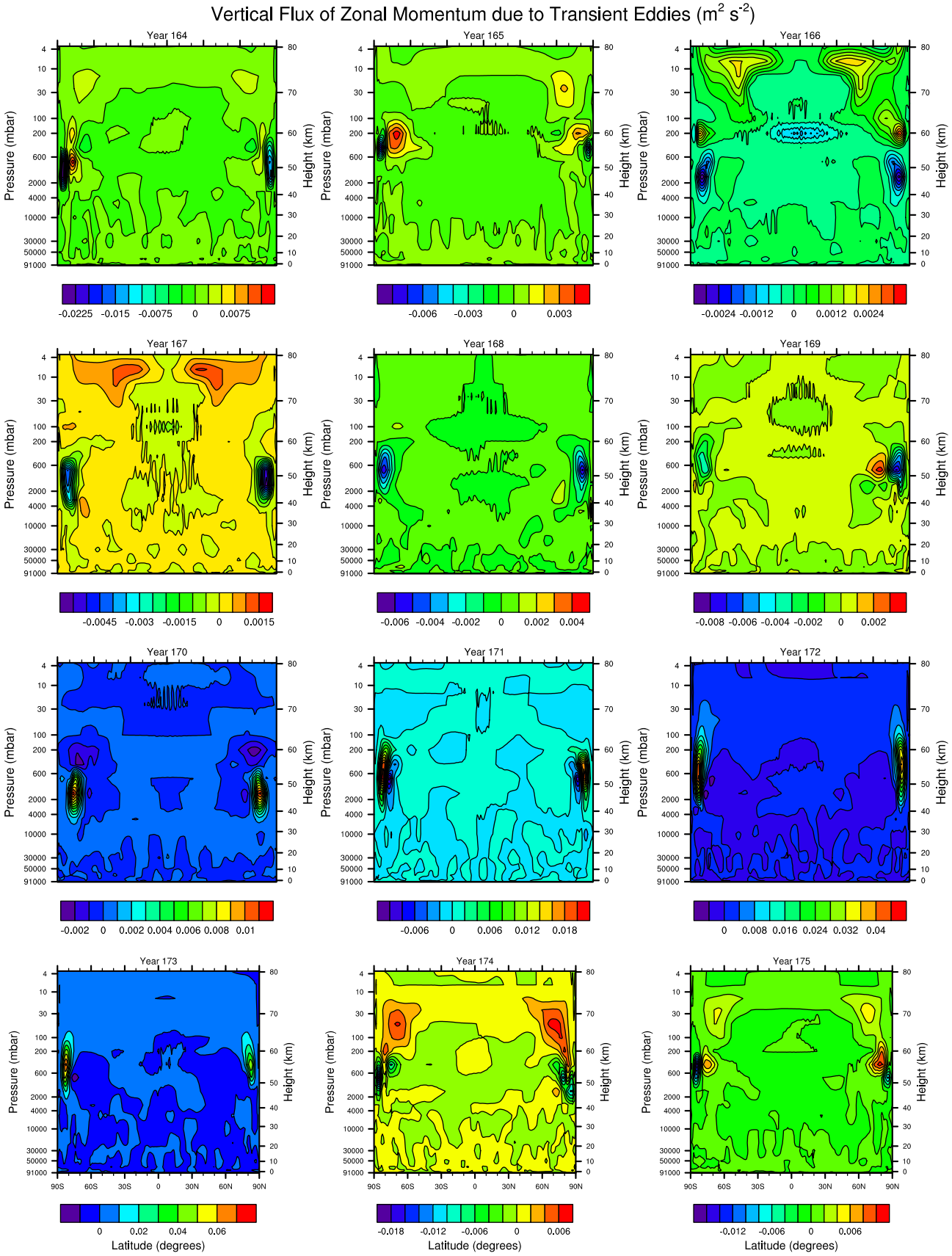

Fig. 14. Zonal mean cross-sections of the vertical flux of zonal angular momentum due to transient eddies (m^2 s^{-2}).

primarily transient eddies in our simulations, transport angular momentum back toward the equator. There is also an overall upward motion of momentum at low latitudes and downward motion of momentum at higher latitudes below around 30 km altitude, although a few small reversals of the generally upward or downward motion are seen at these altitudes.

3.2.2.2. Flux convergences.

3.2.2.2.1. Convergence of meridional flux of zonal angular momentum.

3.2.2.2.1.1. Convergence by time-mean meridional cells. Flux convergences represent the instantaneous rate of accumulation of angular momentum due to fluxes in particular directions. Fig. 15 shows the convergence of the meridional flux of zonal angular momentum due to time-mean meridional cells (in $m^2\ s^{-2}$) given by

$$-1/(R\cos(\varphi))\frac{d}{d\varphi}(R\cos^2(\varphi)[< u >][< v >]) \quad (5)$$

where R = mean planetary radius (Peixoto and Oort, 1992).

Between years 170 and 172 there is a convergence of momentum flux at high latitudes between around 50 and 60 km altitude, which accelerates the westward winds and leads to the buildup of westward wind jets at high latitudes (Fig. 3). These regions of convergence move upward and to higher latitudes in each hemisphere as the zonal wind jets also build up and move upward and to higher latitudes. Between years 164 and 166 there are regions of convergence of the angular momentum flux at high latitudes between around 55 and 60 km altitude that move upward and toward lower latitudes during this interval and correspond to the movement of the westward zonal wind jets upward and toward the equator. There is also convergence closer to the equator at this altitude and above, and a tendency for the regions of convergence to move to higher altitudes during this time interval, associated with a corresponding movement of the westward jets from high latitudes toward the equator and upward in altitude. During years 171–173, negative flux convergences (divergences) of the momentum flux build up close to the poles around 55–60 km altitude, decelerate the westward wind, and are associated with a movement of the westward zonal wind jets away from very high latitudes back toward the equator, as seen in Fig. 3. During years 166–169 there are divergences of momentum flux at high latitudes between around 50 and 60 km altitude. These divergences accelerate the eastward winds and move to higher altitudes during this interval, corresponding to the buildup of the eastward zonal jets at high latitudes. The eastward jets also show an upward movement during this time interval.

3.2.2.2.1.2. Convergence due to transient eddies. Fig. 16 shows the convergence of the meridional flux of zonal angular momentum due to transient eddies (in $m^2\ s^{-2}$) given by $-1/(R\cos(\varphi))\mathrm{d}/\mathrm{d}\varphi\ (R\cos^2(\varphi)[u'v'])$.

The convergences due to eddies are generally a few times smaller than those due to time-mean meridional cells and those due to stationary perturbations are from a few times to an order of magnitude smaller than those due to eddies, so only the convergences due to transient eddies are shown here. In general the flux convergences due to transient eddies act in the opposite sense to the convergences due to time-mean meridional cells.

The momentum flux convergences due to transient eddies, which correspond to acceleration of the westward winds, are seen near the equator around 50–60 km altitude in year 164, as well as in years 174 and 175, corresponding to the movement of the westward wind jets toward the equator. The convergences tend to move upward between years 164 to 166 and between years 174 and 175, corresponding to the upward motion of the region of westward winds above around 60 km altitude during these times. Divergences, which tend to decelerate the westward winds, are also seen at high latitudes around 50–60 km altitude during years 164–166 and years 174–175, and correspond to the movement of the westward wind jets from high latitudes toward the equator during these times (see Fig. 3). During year 170, convergences of momentum flux at high latitudes around 60 km altitude decelerate the eastward winds and reduce the magnitude of the high latitude eastward zonal jets. During years 171–172, convergences of momentum flux at high latitudes around 50–60 km altitude build up the westward zonal wind jets at high latitudes, while divergences of momentum flux close to the poles in the same altitude range oppose the buildup of the high latitude westward zonal wind jets and transport them back toward the equator.

3.2.2.2.2. Convergence of vertical flux of zonal angular momentum.

3.2.2.2.2.1. Convergence by time-mean meridional cells. Fig. 17 shows the convergence of the vertical flux of zonal angular momentum due to time-mean meridional cells (in $m^2\ s^{-2}$) given by $-\mathrm{d}/\mathrm{d}P\ (R\cos(\varphi)[\langle u\rangle][\langle w\rangle])$, where w = vertical velocity in pressure coordinates ($=\mathrm{d}P/\mathrm{d}t$).

The convergences of vertical flux of zonal angular momentum due to time-mean meridional cells are generally an order of magnitude or more larger than the corresponding convergences of meridional flux due to time-mean meridional cells. During years 165 and 169 between around 50 and 60 km altitude there are divergences of the vertical flux of zonal momentum at latitudes below around ±40° and convergences at higher latitudes. These correspond to the regions of upward motion of zonal momentum at low latitudes and downward motion of zonal momentum at higher latitudes associated with the vertical fluxes due to time-mean meridional cells seen in Fig. 13 in the regions of eastward winds. The convergences and divergences maximize toward the top of these regions, corresponding to the tendency of these regions to move upward between years 165 and 169. Similarly, during years 170–171, between around 50 and 60 km altitude there are convergences of the vertical flux of zonal momentum at latitudes below around ±40°, and divergences at higher latitudes. These correspond to the regions of upward motion of zonal momentum at low latitudes and downward motion of zonal momentum at higher latitudes associated with the vertical fluxes due to time-mean meridional cells in the regions of westward winds. The convergences and divergences between 50 and 60 km altitude in years 170–171 also maximize toward the top of these regions, corresponding to the tendency of these regions to move upward during this time interval. During years 170 and 172 there is a divergence of the vertical flux of zonal angular momentum near the equator between around 70 and 75 km altitude. This divergence moves downward during this time interval and corresponds to decreasing westward winds around 75 km altitude at the equator. This corresponds to a movement of the westward wind maximum at the equator downward from around 75 to 65 km altitude during this time interval. During years 164–165 (and years 174–175) above around 60 km altitude there is a convergence of momentum flux near the equator, moving upward with time, consistent with the upward motion of the westward winds between around 60 and 70 km altitude during these times.

3.2.2.2.2.2. Convergence due to transient eddies. Fig. 18 shows the convergence of the vertical flux of zonal angular momentum due to transient eddies (in $m^2\ s^{-2}$) given by $-\mathrm{d}/\mathrm{d}P(R\cos(\varphi)[u'w'])$.

The convergence of the vertical flux of zonal angular momentum by transient eddies tends to be a few times smaller in magnitude than the corresponding flux due to time-mean meridional cells. During years 164–168, between around 75 and 80 km altitude and during years 172–175 between around 70 and 75 km altitude, there are convergences of the vertical flux of zonal momentum due to transient eddies, which accelerate the westward winds at these altitudes and correspond to the upward motion of the westward jets between 60 and 75 km altitude.

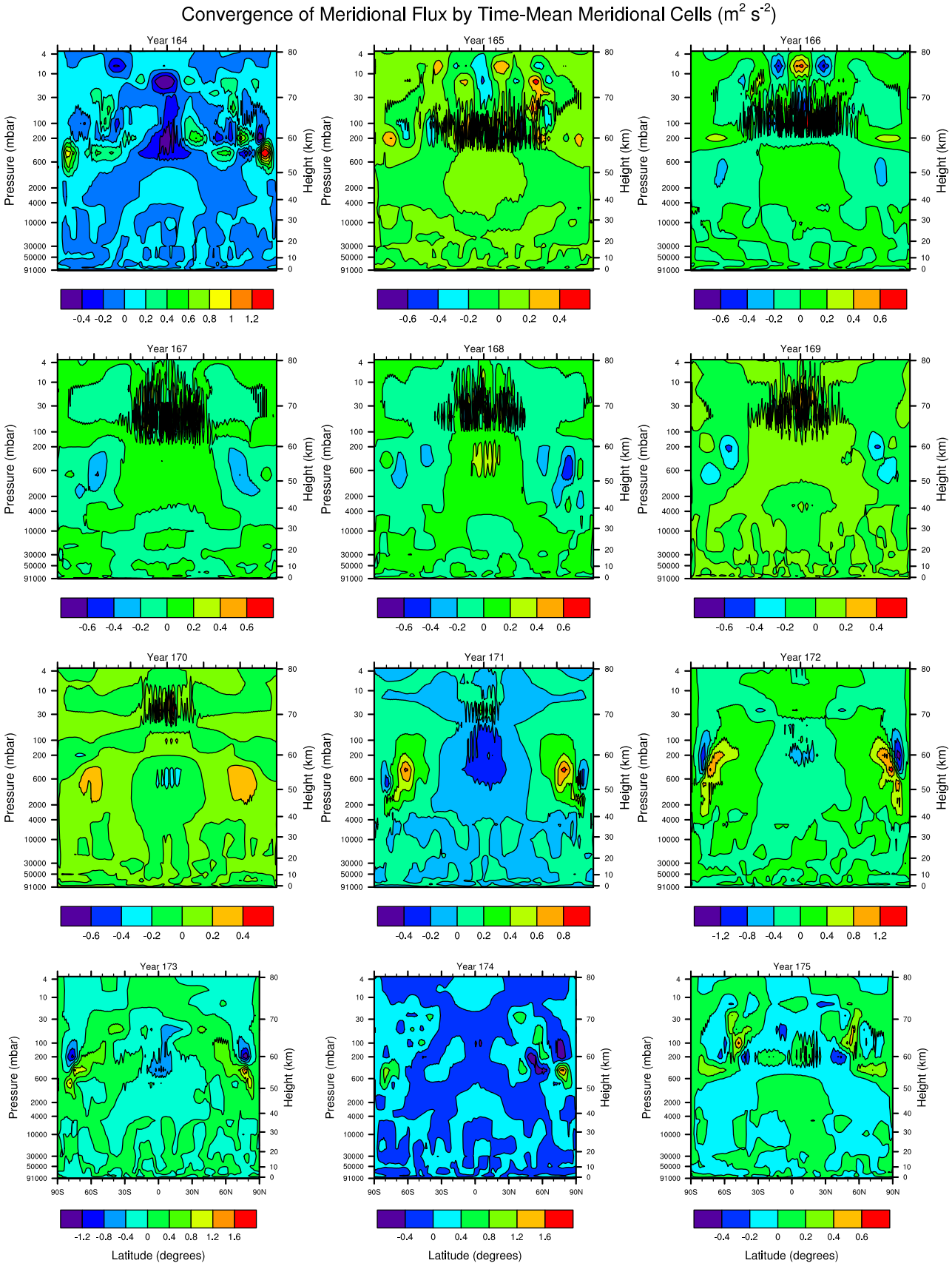

Fig. 15. Convergence of the meridional flux of zonal angular momentum due to time-mean meridional cells ($m^2\,s^{-2}$).

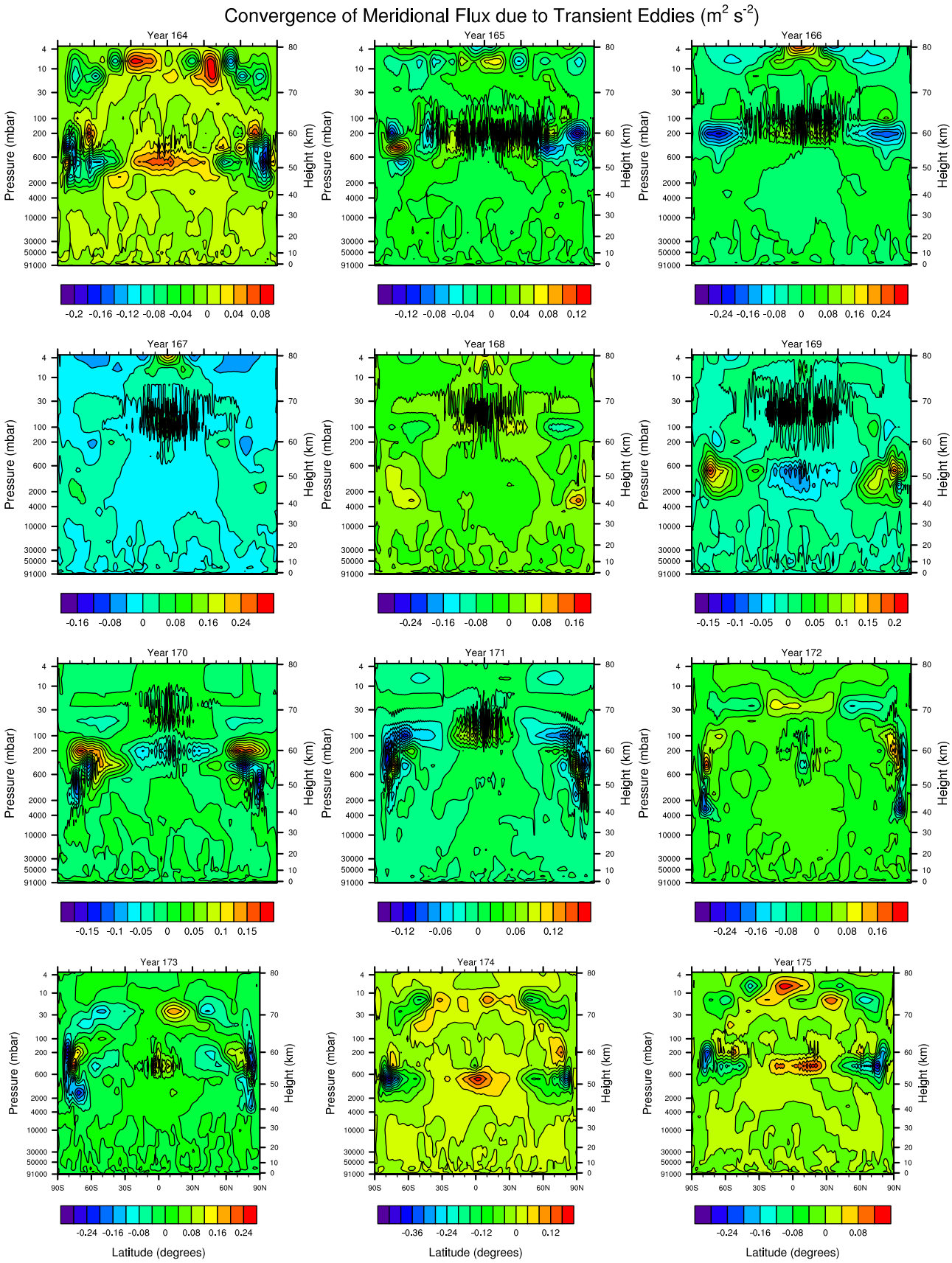

Fig. 16. Convergence of the meridional flux of zonal angular momentum due to transient eddies ($m^2\ s^{-2}$).

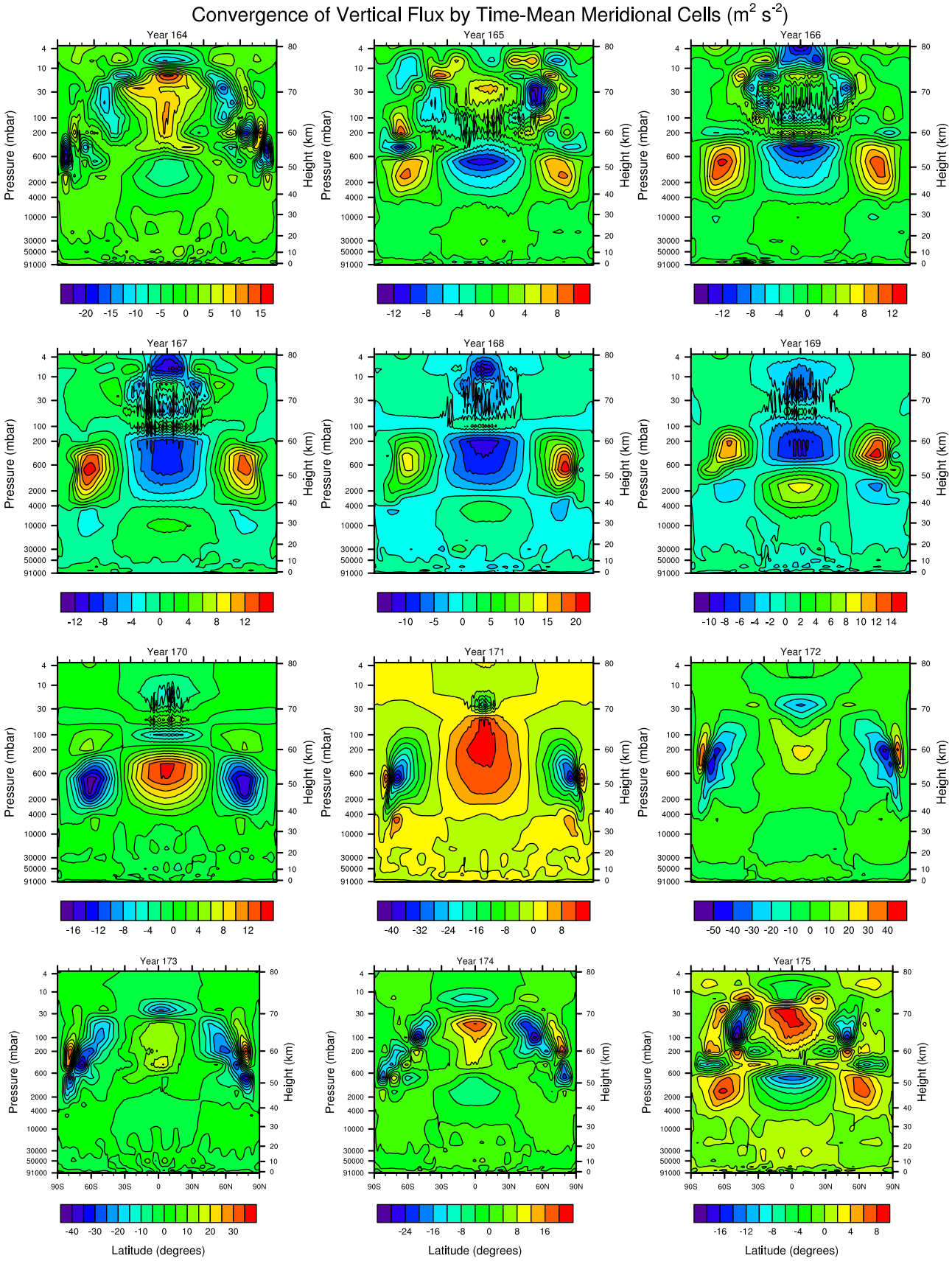

Fig. 17. Convergence of the vertical flux of zonal angular momentum due to time-mean meridional cells ($m^2\ s^{-2}$).

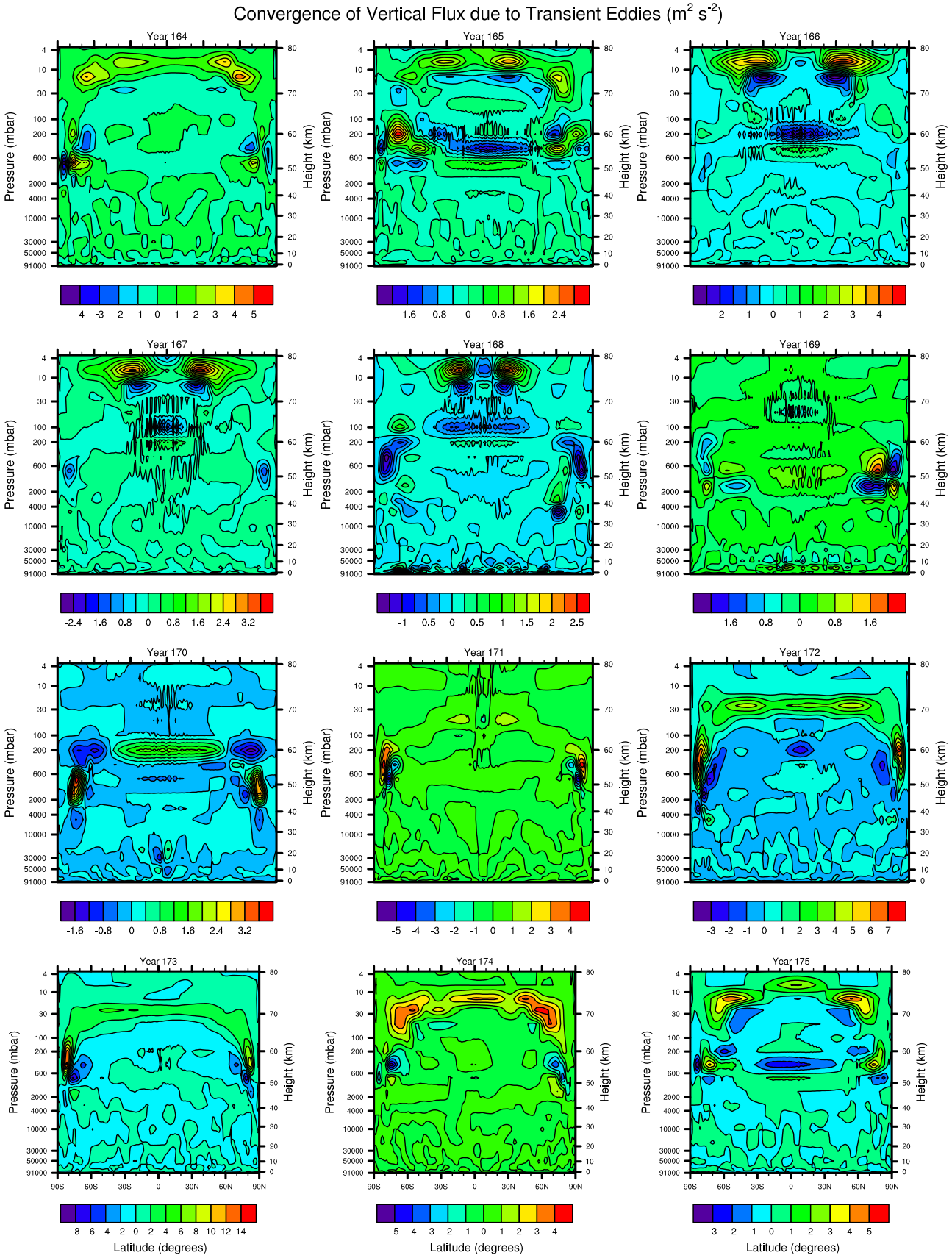

Fig. 18. Convergence of the vertical flux of zonal angular momentum due to transient eddies (m^2 s^{-2}).

Similarly, during years 165–169 there are divergences of the vertical flux of zonal momentum at low latitudes between around 55 and 70 km altitude, that move upward during this interval. These divergences increase the eastward winds at these altitudes and lead to the upward motion of the eastward jets between 30 and 65 km altitude over this time interval. The convergences of the stationary perturbations of the vertical flux of zonal momentum tend to act in the same sense as the eddy flux convergence, but with values around an order of magnitude smaller, and are not shown here.

4. Discussion

Our model simulations generate superrotating long term mean zonal winds with magnitudes at cloud top heights that are within the range of observations from the Venera and Pioneer Venus probes (Schubert et al., 1980; Schubert, 1983). However, our cloud top winds are around 30–50% smaller than cloud-tracking wind observations (Del Genio and Rossow, 1990). Our wind magnitudes are also significantly smaller than those observed below the simulated zonal wind maximum, at altitudes less than about 50 km. Our yearly results display significant regions of subrotation, which have not been found in any measurements to date. However, regions of subrotation in our model occur only below the clouds and there are limited observations of subcloud wind velocities in the Venus atmosphere.

The decadal periodicity exhibited by the model may or may not represent a realistic state of the Venus atmosphere since we have made a number of simplifying assumptions in our simulations, including the simplified radiative forcing, no surface topography, and no diurnal or seasonal cycles. However, the simulated winds represent a possible dynamical state of an atmosphere with the basic characteristics of the Venus atmosphere and physical processes occurring in the simulations could also be present within the real Venus atmosphere. Examination of the circulation and the periodicities in the simulation could help to elucidate the mechanisms responsible for superrotation in the Venus atmosphere.

Our simulations suggest that there is no single simple Hadley cell that transports angular momentum from the surface to cloud top level. Multiple meridional wind reversals and local reversals of the net upward or downward motion are often present at altitudes less than around 40 km. However, a simple Hadley-type circulation occurs within the regions where westward or eastward jets form between around 40 and 65 km altitude. We see evidence of a vacillation cycle in the westward winds, in which mid-latitude jets form in some years and an equatorial maximum forms in other years. We emphasize that the model atmosphere at cloud heights and above is always superrotating though regions of subrotation occur at lower altitudes. At cloud heights and above the superrotating atmosphere oscillates between a state with mid-latitude jets and one without jets but with an equatorial maximum in the zonal wind. Given the present observational data base, it is not possible to rule out sub-cloud regions of subrotating zonal winds at some times in the Venus atmosphere. If our model had produced superrotating winds which were larger in magnitude, it is also possible that the decadal cycle might be present but not produce any net subrotating winds, i.e., the oscillatory momentum exchange with the surface might simply modulate the superrotating flow but not completely reverse it.

Observations suggest that there may be significant variability within the superrotating winds on Venus. Measurements from Mariner 10 (made during early 1974) (Limaye, 1977; Travis, 1978; Limaye and Suomi, 1981), Pioneer Venus (made between 1978 and 1982) (Rossow et al., 1980a; Schubert et al., 1980; Limaye, 2007), and more recent Venus Express measurements (made during 2007) (Markiewicz et al., 2007) suggest possible variations in latitudinal wind structure over time, including differences in the strength of the mid-latitude jets and the latitude of the maximum zonal wind velocities. However, the details of these observations must be treated with caution due to the difficulties inherent in resolving the winds accurately with the available instrumentation and viewing geometries (Limaye, 2007) and possible obscuration of the mid-latitude jets by haze layers (Moissl et al., 2009). Regions of subrotating winds below the cloud deck, such as those we find in our simulations, have not been observed in Venus' atmosphere but, as stated above, such observations are limited in space and time.

Measurements of Venus' atmospheric composition and temperature also suggest the presence of periodicities with multi-year timescales. Ground-based microwave spectral line observations of CO from year 1982 to year 1990 between 75 and 105 km altitude show a significant cyclic variation in both the CO composition and the temperature (Clancy and Muhleman, 1991). Clancy and Muhleman (1991) find that these cyclic variations have a period around 10 years, i.e., they find a decadal variation with approximately the same timescale as the one we produce in our simulations. Our decadal oscillation might provide a possible dynamical source for these observed variations. Clancy and Muhleman (1991) find that the long term variations in their mesospheric temperature measurements are consistent with observations of mesospheric temperatures from Pioneer Venus and Venera probes. Clancy and Muhleman (1991) suggest that variations in the global scale dynamics within and above the cloud layers of Venus' atmosphere may be the source of the observed periodicity.

Long term variations with timescales of the order of tens of years are also found above the cloud tops in SO_2 observations by balloons, rockets, the Hubble Space Telescope, the International Ultra Violet explorer, Pioneer Venus, and Venus Express, over a time interval of around 40 years (Belyaev et al., 2008). The SO_2 content was found to rise sharply between 1967 and 1979, followed by a downward trend between 1979 and 1995. Recent observations from Venus Express show that the SO_2 content has risen again significantly in 2006 and 2007 (Belyaev et al., 2008), suggesting that this may be a cyclic variation rather than a single perturbation, with a period of around 20–25 years. Our decadal oscillation may also provide a possible source for this observed cycle. Belyaev et al. (2008) suggest changes in atmospheric dynamics as a possible cause for the large observed variations in SO_2, as an alternative explanation to changes in eddy diffusion (Krasnopolsky, 1986) or volcanism (Esposito, 1984) which have been suggested previously to explain the observed SO_2 variations.

Oscillations with very long periods of the order of years are common within planetary atmospheres. For example, the quasi-biennial oscillation (QBO) of stratospheric zonal winds is a regularly observed feature within the Earth's atmosphere (Andrews et al., 1987; Baldwin et al., 2001). The decadal oscillations we find in our simulations differ from the QBO. The QBO is understood in terms of Doppler effects causing waves such as gravity waves, which transfer momentum upward, to be preferentially absorbed below the wind maximum, so that the winds are accelerated below the wind maximum, giving downward propagation of the oscillation. For a QBO-like mechanism to force the upward propagation of the zonal wind system on Venus the waves would have to originate above the upward-propagating structure, for which there is no obvious source, or the waves would have to be absorbed above the peak while escaping absorption below, which is not explicable in terms of Doppler effects. A 4.5 (Earth) year periodicity in winds and temperature has been found within the stratosphere of Jupiter (Leovy et al., 1991; Friedson, 1999; Flasar et al., 2004), and a 13–16 (Earth) year oscillation has recently been found on Saturn (Fouchet et al., 2008; Orton et al., 2008). While these oscillations occur within atmospheres with widely varying physical conditions, including radiative heating, diurnal and seasonal variations, etc.,

their presence demonstrates that periodic variations on timescales of several years are possible states of many planetary atmospheres.

Variations with periods of the order of a few years have also been found in model simulations of the Venus atmosphere by other investigators. Variabilities with timescales of less than a year to several years with smaller magnitudes than we find in our simulations are seen at 69 km altitude close to the equator within a 250 (Earth) year time series of zonally averaged zonal winds in simulations by Yamamoto and Takahashi (2007). Within their time-varying winds Yamamoto and Takahashi (2007) find a correlation between the magnitude of the superrotating zonal winds and the strength of the meridional circulation. We also find that the strongest superrotating zonal winds tend to be associated with a larger meridional flow. Changes in the cloud top level zonal wind velocities, in which the maximum superrotating wind varies between a mid-latitude jet structure and a maximum spread across low latitudes, are also found to occur over multi-year time periods within the Laboratoire Meteorologie Dynamique (LMD) Venus model when a simplified radiative forcing is applied, although they do not see associated long period upward propagating oscillations.

Various kinds of waves, with relatively short periods have been observed within the Venus atmosphere. For example, Kelvin waves and Rossby waves have been observed (Del Genio and Rossow, 1990). The oscillations we find do not have the characteristics of either of these kinds of waves. Further investigation is needed to determine the exact nature of the temporal variations seen in our model. Since Venus atmospheric observing campaigns to date have only been of relatively short duration, it is difficult to determine whether such multi-year periodicities are present in the Venus atmosphere. It is important to measure the characteristics of the Venus atmosphere on multi-year timescales to understand the true nature of its superrotation. It is also necessary to acquire more data on the winds in the lower atmosphere.

The CAM model is not specifically designed to conserve angular momentum, and we find that angular momentum is only approximately conserved within our simulations. Commonly, Earth climate models do not conserve angular momentum, as discussed in Shaw et al. (2009). These authors note that for simulations in which there is a relatively "high" upper boundary, where the pressure at the lower boundary is around 10^6 times as large as the pressure at the upper boundary, as is the case in our CAM model simulations, imposition of momentum conservation does not have a significant effect on the simulated results. No extra periodicities were found by Shaw et al. (2009) for model simulations in which momentum conservation was not imposed compared with simulations in which conservation was imposed. Thus there is no reason to think that the oscillations we see are a product of the lack of conservation of angular momentum within the CAM model.

The exact nature of the decadal oscillations we find in our simulations is still uncertain. However, initial investigations have determined that the oscillation shows considerable zonal symmetry in the lowest few model levels, and we find that the condition for a symmetric instability is satisfied at low latitudes at the surface in our simulations. We also see evidence of atmospheric overturning in the levels close to the surface. The oscillation also has characteristics of a vacillation cycle with a periodic exchange in momentum between high and low latitudes. Our calculations of angular momentum fluxes and convergences suggest that the vertical propagation of the zonal wind pattern is related to the vertical transport of momentum. It may be that an internal cycle is excited by a symmetric instability near the surface and propagated and modulated by the mean zonal flow and the horizontal and vertical transports of momentum. Momentum is transferred from the solid planet to the atmosphere via the surface–atmosphere interaction. Superrotational flow near the surface is transported upward primarily by the vertical flux due to time-mean meridional cells. The meridional momentum flux due to time-mean meridional cells transports momentum poleward and the meridional momentum flux due to transient eddies transports momentum back towards the equator. As this process continues, the region of superrotating flow grows in height over time, and continues to be transported upward, eventually reaching cloud level. An instability such as the symmetric instability, coupled with the flow near the surface, produces the opposite phase of the oscillation and angular momentum is transported upward mainly due to time-mean meridional cells, poleward by time-mean meridional cells and back to the equator by transient eddies, transporting a region of eastward winds upward. The exact mechanism will be investigated further in future work. Further investigations will be performed in future work to determine the nature of barotropic or baroclinic eddy processes and whether the observed oscillation is connected with a symmetric instability or with another process, possibly related to atmospheric overturning near the surface.

Maintenance of the superrotation in our Venus atmosphere simulations involves elements of previously described processes, but the complete mechanism operative in our model has not been identified heretofore. In our model angular momentum from the solid planet is fed into the near surface region of the atmosphere and this atmospheric mass rises upward and expands. Our analyses of angular momentum fluxes and convergences show that the meridional circulation within an air mass redistributes the angular momentum and feeds into the formation of the mid-latitude jets. Our analyses show that the jets become unstable, primarily due to the effects of eddies, and to a much smaller extent due to stationary perturbations. The eddies return the angular momentum in the jets equatorward producing a broad superrotating cloud level zonal circulation. A similar process involving subrotating air masses occurs in between intervals of superrotation, but the subrotating air masses have relatively small angular momentum and zonal wind velocities. The net consequence of the periodic processes is to establish a globally superrotating atmosphere. The physics of angular momentum transport in our model is generally consistent with the GRW mechanism as a means of transporting angular momentum to the cloud level. However, our results suggest that this is accomplished not by a single simple Hadley cell between the surface and the cloud level, but that there is a more complex flow within around 40 km of the surface in which there are multiple meridional wind reversals, and some reversals of the net upward or downward motion. We also see a vacillation cycle associated with the upward moving decadal oscillations in which westward jets form in some years and a single equatorward westward maximum forms in other years.

5. Conclusions

With our modified version of the CAM model, including a simplified radiative forcing and other simplifications such as no topography and no seasonal or diurnal cycle, we generate superrotating mean winds that are comparable in magnitude to probe measurements, though smaller than cloud-tracking wind observations. Our wind magnitudes below the cloud top region are significantly smaller than those measured. In our time-dependent results, we find a significant decadal oscillation in the zonal winds, which includes regions of superrotation and regions of smaller subrotating winds traveling upward from the lower boundary. The oscillation also involves a vacillation cycle in which the zonal wind maxima at cloud top heights move periodically from high to low latitudes, alternating between mid-latitude zonal jets and a single equatorial zonal wind maximum. Observations reveal variability in the winds at cloud top heights with timescales of 5–10 years, although the measured variations are only around half the magnitude of the

wind variations we find in our simulations at a similar altitude and latitude. Also, regions of subrotation below the clouds have not been found in measurements to date. Some variability in cloud top wind magnitudes with timescales of several years has been found in other modeling studies, but with smaller magnitudes and these do not appear to have the same characteristics as the oscillation we find in our simulations. The results of our simulations may or may not represent a realistic state of Venus' atmosphere, since we have made a number of simplifying assumptions, but they may elucidate processes which can occur within a Venus-like atmosphere. The exact nature of the oscillation is still uncertain, but may be related to some kind of instability coupled with a periodic overturning process. The winds near the lower boundary show considerable zonal symmetry and we find that the conditions for a symmetric instability to occur are satisfied at the lower boundary at low latitudes. The lowest few atmospheric levels also show evidence of atmospheric overturning.

Analyses of the meridional circulation suggest that the atmospheric circulation does not conform to a simple single large Hadley cell circulation from the surface to cloud top level. The meridional winds show stacked meridional cells in the atmosphere below around 40 km altitude, with alternating meridional wind directions between different layers. However, there may be regions between around 40 and 60 km altitude in which a simple Hadley-type circulation exists together with westward or eastward zonal jets. Calculations of the angular momentum fluxes and convergences show that the time-mean meridional circulation transports zonal angular momentum upward at latitudes within around ±40° of the equator and downward at higher latitudes. Within the altitude regions where mid-latitude zonal jets form, the time mean meridional circulation is found to transport angular momentum to high latitudes where the zonal jets are formed, and waves, primarily transient eddies (and to a much smaller extent stationary perturbations), transport angular momentum back from the jets toward the equator. Our results are generally consistent with the GRW mechanism as a means of transporting momentum to the cloud level. However, our results suggest that this is accomplished not by a single simple Hadley cell between the surface and the cloud level, but that there is a more complex flow within around 40 km of the surface in which there are multiple meridional reversals, and some reversals of the net upward or downward flow. We also find the presence of a vacillation cycle associated with the decadal variations, in which mid-latitude jets appear in some years and a single equatorial maximum is generated in other years, and in which angular momentum is transported periodically from high to low latitudes and back. More long term measurements of Venus' atmosphere are needed to determine the presence of variations in the atmosphere with periods of the order of several to 10 years. More measurements are also needed to better determine the nature of the circulation below cloud top altitudes.

Acknowledgments

HFP, GS, CC, and AG acknowledge support from NASA's Planetary Atmospheres Program through Grant NASA NNX07AF27G. This work was performed in part under the auspices of the Office of Science, US Department of Energy, by the Lawrence Livermore National Laboratory under Contract DE-AC52-07NA27344. RLW acknowledges support from NASA Grant NNX08AM13G.

References

Andrews, D.G., Holton, J.R., Leovy, C.B., 1987. Middle Atmosphere Dynamics. Academic Press, Orlando. 489 pp.

Baker, R.D., Schubert, G., Jones, P.W., 2000a. Convectively generated internal gravity waves in the lower atmosphere of Venus. Part I: No wind shear. J. Atmos. Sci. 57, 184–199.

Baker, R.D., Schubert, G., Jones, P.W., 2000b. Convectively generated internal gravity waves in the lower atmosphere of Venus. Part II: Mean wind shear and wave–mean flow interaction. J. Atmos. Sci. 57, 200–215.

Baldwin, M.P., Gray, L.J., Dunkerton, T.J., Hamilton, K., Haynes, P.H., Randel, W.J., Holton, J.R., Alexander, M.J., Hirota, I., Horinouchi, T., 2001. The quasi-biennial oscillation. Rev. Geophys. 39, 179–230.

Belton, M.J.S. et al., 1991. Images from Galileo of the Venus cloud decks. Science 253, 1531–1536.

Belyaev, D., Korablev, O., Fedorova, A., Bertaux, J.-L., Vandaele, A.-C., Montmessin, F., Mahieux, A., Wilquet, V., Drummond, R., 2008. First observations of SO_2 above Venus' clouds by means of solar occultation in the infrared. J. Geophys. Res. 113, E00B25. doi:10.1029/2008JE003143.

Clancy, R.T., Muhleman, D.O., 1991. Long-term (1979–1990) changes in the thermal, dynamical, and compositional structure of the Venus mesosphere as inferred from microwave spectral line observations of ^{12}CO, ^{13}CO, and $C^{18}O$. Icarus 89, 129–146. doi:10.1016/0019-1035(91)90093-9.

Collins, W.D. et al. 2004. Description of the NCAR Community Atmosphere Model (CAM 3.0). Tech. Rep., National Center for Atmospheric Research, Boulder, CO, Technical Report NCAR/TN–464+STR, 210pp.

Counselman, C.C., Gourevitch, S.A., King, R.W., Loriot, G.B., Ginsberg, E.S., 1980. Zonal and meridional circulation of the lower atmosphere of Venus determined by radio interferometry. J. Geophys. Res. 85, 8026–8030.

Covey, C.C., Schubert, G., 1981. 4-Day waves in the Venus atmosphere. Icarus 47, 130–138.

Covey, C.C., Schubert, G., 1982. Planetary-scale waves in the Venus atmosphere. J. Atmos. Sci. 39, 2397–2413.

Del Genio, A.D., Rossow, W.B., 1990. Planetary-scale waves and the cyclic nature of cloud-top dynamics on Venus. J. Atmos. Sci. 47, 293–318.

Del Genio, A.D., Zhou, W., 1996. Simulations of superrotation on slowly rotating planets: Sensitivity to rotation and initial condition. Icarus 120, 332–343.

Del Genio, A.D., Zhou, W., Eichler, T.P., 1993. Equatorial superrotation in a slowly rotating GCM: Implications for Titan and Venus. Icarus 101, 1–17.

Esposito, L., 1984. Sulfur dioxide: Episodic injection shows evidence for active Venus volcanism. Science 223, 1072–1074.

Eymet, V., Fournier, R., Dufresne, J.-L., Lebonnois, S., Hourdin, F., Bullock, M.A., 2009. Net-exchange parameterization of the thermal infrared radiative transfer in Venus' atmosphere. J. Geophys. Res. 114, E11008. doi:10.1029/2008JE003276.

Fels, S.B., 1977. Momentum and energy exchanges due to orographically scattered gravity waves. J. Atmos. Sci. 34, 499–514.

Fels, S.B., Lindzen, R.S., 1974. The interaction of thermally excited gravity waves with mean flows. Geophys. Fluid Dynam. 6, 149–192.

Flasar, F.M. et al., 2004. An intense stratospheric jet on Jupiter. Nature 427, 132–135.

Fouchet, T., Guerlet, S., Strobel, D.F., Simon-Miller, A.A., Bezard, B., Flasar, F.M., 2008. An equatorial oscillation in Saturn's middle atmosphere. Nature 453, 200–202. doi:10.1038/nature06912.

Friedson, A.J., 1999. New observations and modelling of a QBO-like oscillation in Jupiter's stratosphere. Icarus 137, 34–55. doi:10.1006/icar.1998.6038.

Gierasch, P.J., 1975. Meridional circulation and the maintenance of the Venus atmospheric circulation. J. Atmos. Sci. 32, 1038–1044.

Gierasch, P.J. et al., 1997. The general circulation of the Venus atmosphere: An assessment. In: Bougher, S., Hunten, D., Phillips, R. (Eds.), Venus. II: Geology, Geophysics, Atmosphere, and Solar Wind Environment. University of Arizona Press, Tucson, pp. 459–500.

Gold, T., Soter, S., 1969. Atmospheric tides and the resonant rotation of Venus. Icarus 11, 356–366. doi:10.1016/0019-1035(69)90068-2.

Herrnstein, A., Dowling, T.E., 2007. Effects of topography on the spin-up of a Venus atmospheric model. J. Geophys. Res. 112, E04S08. doi:10.1029/2006JE002804.

Hide, R., 1969. Dynamics of the atmospheres of the major planets with an appendix on the viscous boundary layer at the rigid bounding surface of an electrically-conducting rotating fluid in the presence of a magnetic Field. J. Atmos. Sci. 26, 841–853.

Hollingsworth, J.L., Young, R.E., Schubert, G., Covey, C., Grossman, A.S., 2007. A simple-physics global circulation model for Venus: Sensitivity assessments of atmospheric superrotation. Geophys. Res. Lett. 34, L05202. doi:10.1029/2006GL028567.

Hou, A.Y., Farrell, B.F., 1987. Superrotation induced by critical-level absorption of gravity waves on Venus: An assessment. J. Atmos. Sci. 44, 1049–1061.

Jablonowski, C., Lauritzen, P.H., Taylor, M.A., Nair, R.D., 2008. Intercomparison of 10 atmospheric model dynamical cores. EOS Trans. AGU 89, Fall Meeting Suppl.

Joshi, M., Young, R., 2002. Is the mean venusian tropospheric circulation unsteady? Geophys. Res. Lett. 29, 1062. doi:10.1029/2001GL013979.

Krasnopolsky, V.A., 1986. Photochemistry of the Atmospheres of Mars and Venus. Springer, Heidelberg-New York. 334pp.

Lebonnois, S., Hourdin, F., Eymet, V., Crespin, A., Fournier, R., Forget, F., 2010. Superrotation of Venus' atmosphere analyzed with a full general circulation model. J. Geophys. Res. 115, E06006. doi:10.1029/2009JE003458.

Lee, C., Lewis, S.R., Read, P.L., 2005. A numerical model of the atmosphere of Venus. Adv. Space Res. 36, 2142–2145.

Lee, C., Lewis, S.R., Read, P.L., 2007. Superrotation in a Venus general circulation model. J. Geophys. Res. 112, E04S11. doi:10.1029/2006JE002874.

Leovy, C.B., Friedson, A.J., Orton, G.S., 1991. The quasiquadrennial oscillation of Jupiter's equatorial stratosphere. Nature 354, 380–382. doi:10.1038/354380a0.

Leroy, S.S., Ingersoll, A.P., 1995. Convective generation of gravity waves in Venus's atmosphere: Gravity waves spectrum and momentum transport. J. Atmos. Sci. 52, 3717–3737.

Limaye, S.S., 1977. Venus Stratospheric Circulation: A Diagnostic Study. PhD Thesis, University of Wisconsin, Madison.
Limaye, S.S., 2007. Venus atmospheric circulation: Known and unknown. J. Geophys. Res. 112, E04S09. doi:10.1029/2006JE002814.
Limaye, S.S., Suomi, V.E., 1981. Cloud motions on Venus: Global structure and organization. J. Atmos. Sci. 38, 1220–1235.
Limaye, S.S., Grassoti, C., Kuetemeyer, M.J., 1988. Venus: Cloud level circulation during 1982 as determined from pioneer cloud photopolarimeter images : I. Time and zonally averaged circulation. Icarus 73, 193–211. doi:10.1016/0019-1035(88)90093-0.
Lin, S.-J., Rood, R.B., 1996. Multidimensional flux form semi-Langrangian transport schemes. Mon. Weath. Rev. 124, 2046–2070.
Lin, S.-J., Rood, R.B., 1997. An explicit flux-form semi-Langrangian shallow water model on the sphere. Q. J. R. Meteorol. Soc. 123, 2531–2533.
Markiewicz, M.J., Titov, D.V., Limaye, S.S., Keller, H.U., Ignatiev, N., Jaumann, R., Thomas, N., Michalik, H., Moissl, R., Russo, P., 2007. Morphology and dynamics of the upper cloud layer of Venus. Nature 450, 633–636. doi:10.1038/nature06320.
Marov, M.Y., Avduevski, V.S., Kerzhano, V., Rozhdest, M., Borodin, N.F., Ryabov, O.L., 1973. Venera 8-measurements of temperature, pressure and wind velocity on illuminated side of Venus. J. Atmos. Sci. 30, 1210–1214.
Moissl, R. et al., 2009. Venus cloud top winds from tracking UV features in Venus Monitoring Camera images. J. Geophys. Res. 114, E00B31. doi:10.1029/2008JE003117.
Murray, B.C., Belton, M.J.S., Danielson, G., Davies, M.E., Gault, D., Hapke, B., Oleary, B., Strom, R.G., Suomi, V., Trask, N., 1974. Venus: Atmospheric motion and structure from Mariner 10 pictures. Science 183, 1307–1315.
Newman, M., Leovy, C.B., 1992. Maintenance of strong rotational winds in Venus' middle atmosphere by thermal tides. Science 257, 647–650.
Newman, M., Schubert, G., Kliore, A.J., Patel, I.R., 1984. Zonal winds in the middle atmosphere of Venus from Pioneer-Venus radio occultation data. J. Atmos. Sci. 41, 1901–1913.
Orton, G.S. et al., 2008. Semi-annual oscillations in Saturn's low-latitude stratospheric temperatures. Nature 453, 196–199. doi:10.1038/nature06897.
Pechman, J.B., Ingersoll, A.P., 1984. Thermal tides in the atmosphere of Venus: Comparison of model results with observations. J. Atmos. Sci. 41, 3290–3313.
Peixoto, J.P., Oort, A.H., 1992. Physics of Climate. American Institute of Physics, New York. 520pp.
Rossow, W.B., 1983. A general circulation model of a Venus-like atmosphere. J. Atmos. Sci. 40, 273–302.
Rossow, W.B., Williams, G.P., 1979. Large-scale motion in the Venus stratosphere. J. Atmos. Sci. 36, 377–389.
Rossow, W.B., Del Genio, A.D., Limaye, S.S., Travis, L.D., Stone, P.H., 1980a. Cloud morphology and motions from Pioneer Venus images. J. Geophys. Res. 85, 8107–8128.
Rossow, W.B., Fels, S.B., Stone, P.H., 1980b. Comments on 'A three-dimensional model of dynamical processes in the Venus atmosphere'. J. Atmos. Sci. 37, 250–252.
Rossow, W.B., Del Genio, A.D., Eichler, T., 1990. Cloud-tracked winds from Pioneer Venus OCPP images. J. Atmos. Sci. 47, 2053–2084.
Schneider, T., 2006. The general circulation of the atmosphere. Annu. Rev. Earth Planet. Sci. 34, 655–688.
Schubert, G., 1983. General circulation and the dynamical state of the Venus atmosphere. In: Hunten, D., Colin, L., Donahue, T., Moroz, V. (Eds.), Venus. University of Arizona Press, Tucson, pp. 681–765.
Schubert, G., Whitehead, J., 1969. The moving flame experiment with liquid mercury: Possible implications for the Venus atmosphere. Science 163, 71–72.
Schubert, G. et al., 1980. Structure and circulation of the Venus atmosphere. J. Geophys. Res. 85, 8007–8025.
Seiff, A., 1983. Thermal structure of the atmosphere of Venus. In: Hunten, D.M., Colin, L., Donahue, T.M., Moroz, V.I. (Eds.), Venus. University of Arizona Press, Tucson, pp. 215–279.
Seiff, A., Kirk, D.B., Young, R.E., Blanchard, R.C., Findlay, J.T., Kelly, G.M., Sommer, S.C., 1980. Measurements of thermal structure and thermal contrasts in the atmosphere of Venus and related dynamical observations: Results from the four Pioneer Venus probes. J. Geophys. Res. 85, 7903–7933.
Shaw, T.A., Sigmond, M., Shepherd, T.G., Scinocca, J.F., 2009. Sensitivity of simulated climate to conservation of momentum in gravity wave drag parameterization. J. Clim. 22, 2726–2742. doi:10.1175/2009JCl2688.1.
Simmons, A.J., Strufing, R., 1981. An Energy and Angular-Momentum Conserving Finite-difference Scheme, Hybrid Coordinates and Medium-range Weather Prediction. Tech. Rep., European Centre for Medium-Range Weather Forecasts, ECMWF Technical Report No. 28, 68pp.
Suomi, V.E., 1974. Cloud motions on Venus. In: Hansen, J. (Ed.), The Atmosphere of Venus. Goddard Institute of Space Studies, New York, NY, pp. 42–58.
Takagi, M., Matsuda, Y., 2007. Effects of thermal tides on the Venus atmospheric superrotation. J. Geophys. Res. 112, D09112. doi:10.1029/2006JD007901.
Tomasko, M.G., Doose, L.R., Smith, P.H., Odell, A.P., 1980. Measurements of the flux of sunlight in the atmosphere of Venus. J. Geophys. Res. 85, 8167–8186.
Travis, L.D., 1978. Nature of the atmospheric dynamics on Venus from power spectrum analysis of Mariner 10 images. J. Atmos. Sci. 35, 1584–1595.
Webster, P.J., Keller, J.L., 1975. Atmospheric variations: Vacillations and index cycles. J. Atmos. Sci. 32, 1283–1300.
Yamamoto, M., 2001. Blocky markings and planetary-scale waves in the equatorial cloud layer of Venus. J. Atmos. Sci. 58, 365–375.
Yamamoto, M., Takahashi, M., 2003a. Superrotation and equatorial waves in a T21 Venus-like AGCM. Geophys. Res. Lett. 30, 1449. doi:10.1029/2003GL016924.
Yamamoto, M., Takahashi, M., 2003b. The fully developed superrotation simulated by a general circulation model of a Venus-like atmosphere. J. Atmos. Sci. 60, 561–574.
Yamamoto, M., Takahashi, M., 2004. Dynamics of Venus' superrotation: The eddy momentum transport processes newly found in a GCM. Geophys. Res. Lett. 31, L09701. doi:10.1029/2004GL019518.
Yamamoto, M., Takahashi, M., 2006. Superrotation maintained by meridional circulation and waves in a Venus-like AGCM. J. Atmos. Sci. 63, 3296–3314.
Yamamoto, M., Takahashi, M., 2007. A parametric study of atmospheric superrotation on Venus-like planets: Effects of oblique angle of planetary rotation axis. Geophys. Res. Lett. 34, L16202. doi:10.1029/2007GL030220.
Yamamoto, M., Takahashi, M., 2009. Dynamical effects of solar heating below the cloud layer in a Venus-like atmosphere. J. Geophys. Res. 114, E12004. doi:10.1029/2009JE003381.
Young, R.E., Pollack, J.B., 1977. A three-dimensional model of dynamical processes in the Venus atmosphere. J. Atmos. Sci. 34, 1315–1351.
Young, R.E., Pollack, J.B., 1980. Reply. J. Atmos. Sci. 37, 253–254.
Zasova, L.V., Ignatiev, N., Khatuntsev, I., Linkin, V., 2007. Structure of the Venus atmosphere. Planet. Space Sci. 55, 1712–1728. doi:10.1016/j.pss.2007.01.011.